Nonlinear Dyn (2022) 108:2045–2074
https://doi.org/10.1007/s11071-022-07325-6

ORIGINAL PAPER

Elastic-bound conditions for energetically optimal elasticity and their implications for biomimetic propulsion systems

Arion Pons · Tsevi Beatus

Received: 14 September 2021 / Accepted: 19 February 2022 / Published online: 22 March 2022

Abstract Minimising the energy consumption associated with periodic motion is a priority common to a wide range of technologies and organisms. These include many forms of biological and biomimetic propulsion system, such as flying insects. Linear and nonlinear elasticity can play an important role in optimising the energetic behaviour of these systems, via linear or nonlinear resonance. However, existing methods for computing energetically optimal nonlinear elasticities struggle when actuator energy regeneration is imperfect: when the system cannot reuse work performed on the actuator, as occurs in many realistic systems. Here, we develop a new analytical method that overcomes these limitations. Our method provides exact nonlinear elasticities minimising the mechanical power consumption required to generate a target periodic response, under conditions of imperfect energy regeneration. We demonstrate how, in general parallel- and series-elastic actuation systems, imperfect regeneration can lead to a set of non-unique optimal nonlinear elasticities. This solution space generalises the energetic properties of linear resonance, and is described completely via bounds on the system work loop: the elastic-bound conditions. The choice of nonlinear elasticities from within these bounds leads to new tools for systems design, with particular relevance to biomimetic propulsion systems: tools for controlling the trade-off between actuator peak power and duty cycle; for using unidirectional actuators to generate energetically optimal oscillations; and further. More broadly, these results lead to new perspectives on the role of nonlinear elasticity in biological organisms, and new insights into the fundamental relationship between nonlinear resonance, nonlinear elasticity, and energetic optimality.

Keywords Energetic optimality · Biomimetic propulsion · Nonlinear elasticity · Inverse problem · Global resonance · Flapping-wing flight

A. Pons (✉) · T. Beatus (✉)
The Silberman Institute of Life Sciences, Hebrew University of Jerusalem, Giv'at Ram, Jerusalem, Israel
e-mail: arion.pons@mail.huji.ac.il

T. Beatus
e-mail: tsevi.beatus@mail.huji.ac.il

A. Pons · T. Beatus
The Benin School of Computer Science and Engineering, Hebrew University of Jerusalem, Giv'at Ram, Jerusalem, Israel

1 Introduction

Periodic motion is ubiquitous, in both natural and manufactured systems. In many cases, this motion is intentional—driven by an actuator, and powered by a source of energy—and in such cases, the question of how to minimise the consumption of this energy often

manifests. In studies of biological and biomimetic locomotion systems, for instance, the question of how energy consumption is minimised is highly relevant: in aquatic animals [1–7]; microorganisms [8, 9]; flapping-wing robots [10–12] and insects [13–19]; robotic, prosthetic, and biological limb joints [20–24]; and further. These studies are united by another commonality: in each, energetic optimality is connected with structural resonance: the phenomenon in which structural elasticity, linear or nonlinear, absorbs the system's inertial loads. However, in many of these systems, the precise interplay between resonance, energetic optimality, and nonlinear elasticity is still unclear [16].

A complex ecosystem of contexts, methods and approaches exist in the study of this interplay. Even in simple systems, a range of system-actuator architectures exist, including parallel-elastic actuation (PEA) [25–27], series-elastic actuation (SEA) [22–24, 28], and hybrid forms [29]. A wide range of actuator types are also available. In engineering systems, electromechanical actuators are widespread [30, 31], but pneumatic [32, 33], hydraulic [34], and more exotic actuator types [35, 36] are also used. In biological systems, muscular actuators take many different forms [37, 38]. Each of these actuators can be modelled in various ways, with attendant assumptions, cost functionals, and constraints. In the context of energy optimisation, cost functionals may include mechanical power metrics, in addition to further actuator-specific metrics (e.g. electrical, metabolic) [22–24, 39, 40]. Metrics related to the actuator capability may be used as cost functionals and/or constraints: peak power, peak loads, and metrics of actuator motion [22–24, 41]. And finally, to solve the optimisation problem, a range of methods are available. Natural dynamics approaches are intuitive [25–28], but are restricted in their ability to handle complex problems and seek specified objectives. Convex optimisation approaches are powerful, widely applicable, and can find robust non-parametric solutions in presence of uncertainty [22–24]. However, when the cost functional is non-convex, these approaches can struggle: they are unable to distinguish global minima from local minima; and if the global minimum itself is non-unique, they are unable to give a complete description of this non-unique solution space. One practical situation in which non-convexity and non-uniqueness can arise is the case of imperfect actuator energy regeneration (imperfect backdrive), in which the actuator is unable to perfectly re-convert work done by the system on the actuator back into fuel, or stored energy [25, 39, 40]. An assumption of perfect energy regeneration can be accurate for certain electrical actuators and circuit configurations [25, 42], but regeneration is imperfect, or even non-existent, in many forms of non-electrical actuator (e.g. muscles and internal combustion engines).

In this work, we address several of these limitations with a new contribution to the ecosystem of energy optimisation methods. We develop a new theoretical technique for the analysis of the energetic behaviour of nonlinear systems: a technique analogous to phase-portrait methods [43, 44], but operating on system work loops. Using this technique, we present general and constructive proofs of the solutions to several single-degree-of-freedom (1DOF) actuator-agnostic problems in minimising actuator mechanical power consumption. These proofs describe the optimal nonlinear elasticities and associated actuator load waveforms that minimise actuator power consumption, under conditions of imperfect energy regeneration. They allow for near-arbitrary periodic reference trajectories as well as near-arbitrary time-invariant system dynamics and do not rely on the calculus of optimisation. We show that the resulting optimal nonlinear elasticities are non-unique and are completely described by a set of bounds within the space of elasticity: the elastic-bound conditions. On a methodological level, this constructive-proof approach is distinct from both classical natural dynamics and convex-optimisation approaches to energy optimisation. However, it can interface with convex-optimisation methods by providing an initial pool of solutions, or search space, which can be refined with additional objectives and constraints.

Our results also have a constellation of further theoretical and practical implications. On the practical side, we show how these general optimal solutions include classes of optimal bistable system, optimal unidirectional-drive system, and further systems of industrial relevance. We show how their non-uniqueness yields the ability to shape the system design such that actuator load and power waveform properties (peak power, duty cycle, etc.) match desired characteristics. And we illustrate how, and under what circumstances, the optimality of these solutions propagates through the actuator drivetrain; from optimality

in mechanical power; to optimality in terms of electrical, chemical, or metabolic power. Our results have particular relevance to biological and biomimetic propulsion systems, such as flapping-wing micro-air-vehicles (FW-MAVs) [10–12, 45–48]: they describe energetically optimal ways to use non-conventional actuators (e.g. combustion engines [49]) for flapping-wing flight and suggest new interpretations of the functional morphology of nonlinear elasticity within insect flight motors. On the theoretical side, we find that the optimality problem that we consider, and its solutions, are fundamentally related to several characteristics of nonlinear resonance [50–53]. Through these results, we are able to construct a novel class of non-unique nonlinear resonant state, representing an energy-based generalisation of linear resonance. To our knowledge, the existence of these non-unique states, and their relationship to optimal system design, has not previously been recognised. Our analysis not only contributes general solutions to a difficult energy optimisation problem, but also contributes novel designs for energetically optimal biomimetic propulsion systems using non-conventional actuators and elucidates a fundamental relationship between nonlinear resonance, nonlinear elasticity, and energetic optimality.

2 Elastic-bound conditions

2.1 Metrics of mechanical power

In the drivetrain of a general actuated system, power flows from some designated source (e.g. an electrical cell, or biological metabolism) to some designated output (e.g. the flow of a fluid). Figure 1. A shows a schematic. For a single-degree-of-freedom (1DOF) actuator undergoing periodic motion, over periodic window $t \in [0, T]$, the time-domain mechanical power requirement is $P(t) = F(t)\dot{x}(t)$, for actuator force $F(t)$ and displacement $x(t)$. This power requirement, $P(t)$, may contain regions of both positive ($P > 0$) and negative ($P < 0$) power. Under our convention, positive power ($P > 0$) represents power flow from actuator to system and negative power ($P < 0$), vice-versa. By definition, areas of positive power represent

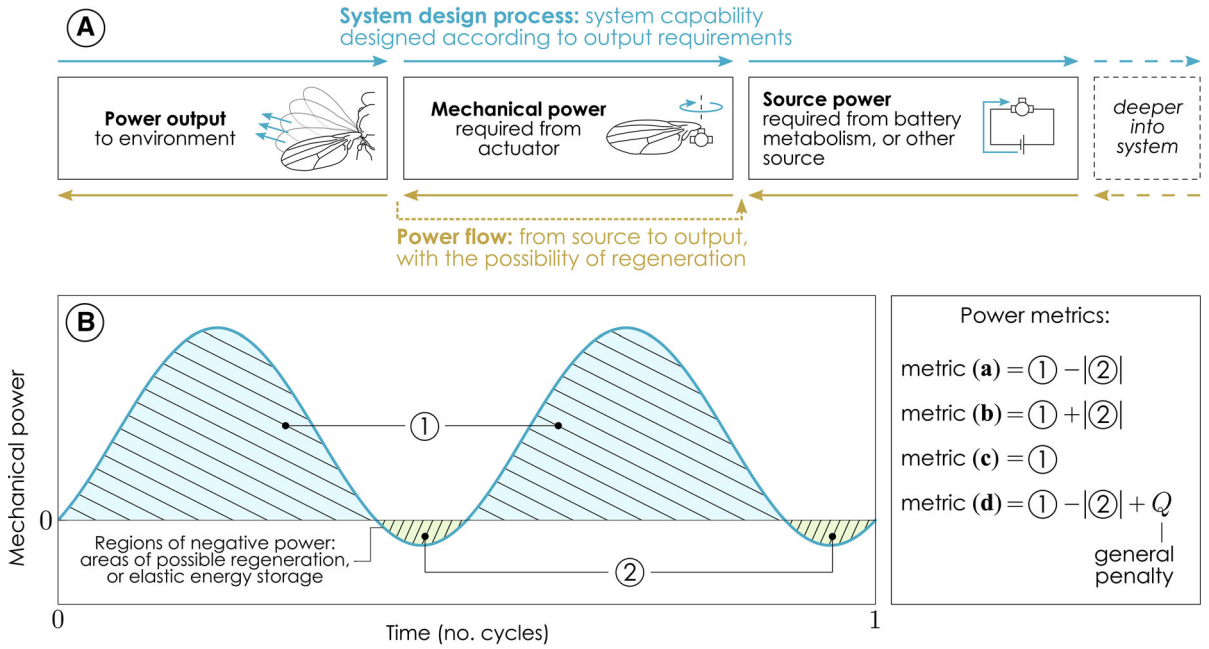

Fig. 1 General system power behaviour. (**A**) Schematic of system power flow: power typically flows from energy source to actuator, with the possibility of energy regeneration in the reverse direction, depending on the system and actuator configuration. The system design process also typically proceeds in the reverse direction: from desired output, to required input. (**B**) Visualisation of general periodic mechanical power requirement $P(t)$, with overall metrics (**a**)–(**d**). Areas of positive (1) and negative (2) power are indicated, as are their effect on the four overall mechanical power metrics

an unavoidable power requirement for the actuator but the implications of negative power are actuator-specific [40, 54, 55]: must the actuator provide this power? Can it dissipate it? Can it store it and thereby regenerate its energy source? In light of these questions, four broad metrics of overall mechanical power consumption, $\overline{\mathrm{P}}_{(\cdot)}$ can be identified:

Metric (**a**): the net power:

$$\overline{P}_{(a)} = \frac{1}{T}\int_0^T P(t)\mathrm{d}t. \tag{1}$$

The net power credits negative power ($P<0$) directly against positive power ($P>0$). It describes the overall system energy dissipation: the power consumption of an actuator with perfect energy regeneration. For some actuators, e.g. certain electrical actuators, with appropriate power electronics [42, 56], assuming perfect regeneration may be admissible. For others, e.g. muscles and combustion engines, the irreversibility of the actuation process precludes any form of regeneration.

Metric (**b**): the absolute power:

$$\overline{P}_{(b)} = \frac{1}{T}\int_0^T |P(t)|\mathrm{d}t, \tag{2}$$

representing the case in which an actuator must provide positive and negative power at full energetic cost. Consider vehicles actuated solely by reaction engines, e.g. rockets or hydrojets: the positive power of acceleration and the negative power of braking must both be provided by the engine. This describes several other robotic [41, 57] and biomechanical [39, 58, 59] systems. However, in other systems, negative power may incur a lesser cost [40], hence:

Metric (**c**): the positive-only power:

$$\overline{P}_{(c)} = \frac{1}{T}\int_0^T P(t)[P(t)\geq 0]_{\mathbb{I}}\mathrm{d}t, \tag{3}$$

where $[\cdot]_{\mathbb{I}}$ is the Iverson bracket, with $[\lambda]_{\mathbb{I}}=1$ for a true statement λ, and $[\lambda]_{\mathbb{I}}=0$ for a false statement λ [60]. The use of this metric implies that the system contains some mechanism or controller to dissipate, but not store or regenerate, negative power. Consider a vehicle with dissipative braking: controlled brake friction dissipates all negative power. This describes several models of insect flight motors [54, 61, 62], and bipedal walking [63].

A general metric, (**d**), can be defined, encompassing metrics (**a**)–(**c**), and a range of other imperfect energy regeneration behaviour, with single penalty function:

$$\overline{P}_{(d)} = \frac{1}{T}\int_0^T \big(P(t)+Q(t)|P(t)|[P(t)\leq 0]_{\mathbb{I}}\big)\mathrm{d}t, \tag{4}$$

for penalty function $Q(t)>0$, $\forall t$, penalising regions of negative power ($P<0$). This general metric allows us to derive a highly generalised results: metrics (**a**)–(**c**) correspond to the choice of particular constant penalties:

$$(\mathbf{a})\ Q=0,\ (\mathbf{b})Q=2,\ (\mathbf{c})\ Q=1. \tag{5}$$

Other models of metabolic energetic cost [64–66] are equivalent to constants $Q=1.33$ and $Q=1.20$. All these metrics represent differing forms of imperfect energy regeneration.

2.2 Optimality in parallel-elastic actuation (PEA) systems under imperfect regeneration

The effect of elasticity on mechanical power metrics (**b**)–(**d**) is system-dependent. Consider a general nonlinear time-invariant single-degree-of-freedom (1DOF) parallel-elastic actuation (PEA) system: an actuator and an elastic element are linked to the system in parallel (Fig. 2). For a system with general Newtonian dynamics $D(\cdot)$, the equations of motion read:

$$\begin{aligned} G(t) &= D(x,\dot{x},\ddot{x},\ldots), \quad \text{without elasticity}\\ F(t) &= D(x,\dot{x},\ddot{x},\ldots)+F_s(x), \quad \text{with elasticity,}\end{aligned} \tag{6}$$

where $F(t)$ and $G(t)$ are the actuator loads with and without elasticity, respectively; $x(t)$ is system displacement (or, kinematic output); and $F_s(x)$ is the elastic profile, dependent only on x. The general dynamical formulation, $D(\cdot)$, allows the treatment of different forms of time-invariant linear and nonlinear system (Fig. 2).

We take the kinematic output, or reference trajectory [22, 23], $x(t)$, as prescribed. It is periodic with period T, and extrema $x_1=\min x$, $x_2=\max x$. This generates an inverse problem: $D(\cdot)$ can be computed directly, and the actuator load $G(t)$ can be visualised in load–displacement space (x-G: abscissa x, ordinate G).

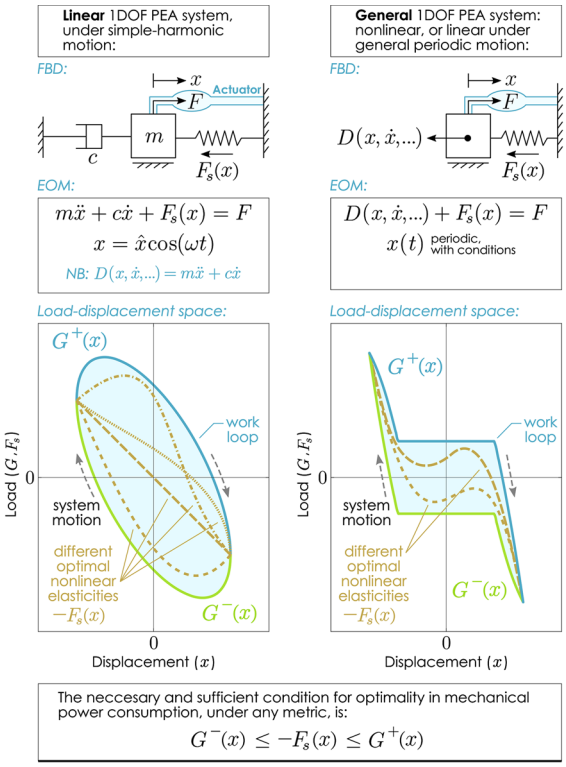

Fig. 2 Elastic-bound conditions in PEA systems. Free-body diagrams (FBD) and equations of motion (EOM) for linear and nonlinear PEA systems. The elastic-bound conditions (Eq. 10) are illustrated on representative work loops in both cases, alongside multiple examples of different optimal nonlinear elasticities. Note that, in our convention, $F_s(x)$ is identified as the elastic action load: the load required to generate deformation. $-F_s(x)$ can correspondingly be identified as the elastic reaction load: the reaction load against deformation

This reveals the system work loop: in load–displacement space, area, $dx \cdot dF$, is mechanical work [37, 67]. The system time-invariant dynamics $D(\cdot)$, and periodic output, $x(t)$, can be arbitrary, except for a few conditions. The inelastic work loop—the loop of $G(t)$—must be a closed simple curve (i.e. no self-intersection), no more than bivalued at any $x \in [x_1, x_2]$, and it must represent net power dissipation (i.e. the progression of time must represent clockwise travel around the closed loop). These conditions are satisfied, e.g. in any system (**i**) with positive linear inertia; (**ii**) with positive linear or nonlinear dissipation; and (**iii**) where $x(t)$ is composed of two half-cycles that are each monotonic.

Under these conditions, we may segment the inelastic work loop, the loop of $G(t)$, into upper (G^+) and lower (G^-) single-valued curves, associated with separate oscillatory half cycles (Fig. 2). These, in turn, generate upper (F^+) and lower (F^-) single-valued curves associated with the elastic work loop—the loop of $F(t)$. Both pairs of curves can be defined with a midline (G_{mid}) and half-width (G_{arc}) component, such that:

$$G^{\pm}(x) = G_{\text{mid}}(x) \pm G_{\text{arc}}(x),$$
$$F^{\pm}(x) = G_{\text{mid}}(x) \pm G_{\text{arc}}(x) + F_s(x) = G^{\pm}(x) + F_s(x). \tag{7}$$

over $x \in [x_1, x_2]$, and where $G_{\text{arc}}(x) \geq 0$, $\forall x$. Under a change of variables ($dx = \dot{x} \cdot dt$7), the mechanical power consumption metrics (**a**)–(**d**) can then be expressed in terms of the loop parameters in equation:

$$\overline{\mathrm{P}}_{(\mathrm{a})} = \frac{1}{T}\int_{x_1}^{x_2} (F^+ - F^-)dx,$$
$$\overline{\mathrm{P}}_{(\mathrm{b})} = \frac{1}{T}\int_{x_1}^{x_2} (|F^+| + |F^-|)dx,$$
$$\overline{\mathrm{P}}_{(\mathrm{c})} = \frac{1}{T}\int_{x_1}^{x_2} \left(F^+[F^+ \geq 0]_{\Vert} - F^-[F^- \leq 0]_{\Vert}\right)dx,$$
$$\overline{\mathrm{P}}_{(\mathrm{d})} = \frac{1}{T}\int_{x_1}^{x_2} \left(F^+ - F^- + Q^+|F^+|[F^+ \leq 0]_{\Vert} + Q^-|F^-|[F^- \geq 0]_{\Vert}\right)dx, \tag{8}$$

where $Q^{\pm}(x) > 0$ are power penalty functions as per the metric (**d**). As per Eqs. 4, 5, metrics (**a**)–(**c**) are a particular form of metric (**d**), with the penalties:

$$\text{(a) } Q^{\pm} = 0, \text{ (b) } Q^{\pm} = 2, \text{ (c) } Q^{\pm} = 1. \tag{9}$$

Finally, we may pose the optimisation problem. Given $x(t)$, what are the elastic profiles, $F_s(x)$, such that the imperfectly regenerated mechanical power consumption, metrics (**b**)–(**d**), is minimised? A simple answer exists:

$$G^-(x) \leq -F_s(x) \leq G^+(x). \tag{10}$$

Equation 10 is the sole criterion, necessary and sufficient, for optimality in metrics (**b**)–(**d**). That is, any sign-flipped nonlinear elastic load profile $-F_s(x)$ that lies within the bounds of the inelastic work loop, $G^{\pm}(x)$, is optimal in mechanical power consumption, irrespective of the penalties associated with negative power. Figure 2 shows a schematic of these conditions, in linear and general nonlinear PEA systems.

Equation 10 is a powerful and general result that allows us to construct a wide range of energetically optimal systems. A full proof, as well as a derivation of $G^{\pm}(x)$ in specific cases, is presented in "Appendix (A.1, A.3)". As an aid to understanding, however, an intuitive, geometric, explanation can be made (Fig. 3). This explanation may be summarised in the following three-step process:

2.2.1 *Step 1: The absence of negative power leads to equality among power metrics*

Negative power arises when the actuator load, $G(t)$ or $F(t)$, and velocity, $\dot{x}(t)$, have opposite sign. In equivalent work-loop terms, negative power arises when the upper loop curve, $G^{+}(x)$ or $F^{+}(x)$, becomes negative; or the lower curve, $G^{-}(x)$ or $F^{-}(x)$, becomes positive. As per Eqs. 8, 9, this negative power is associated with penalties in power metrics (**b**)–(**d**) (Fig. 3A). Because these penalties are dependent on the existence of negative power, if any given loop contains no regions of negative power, then, for that loop, all metrics (**a**)–(**d**) are equivalent: $\overline{\mathrm{P}}_{(\mathrm{a})} = \overline{\mathrm{P}}_{(\mathrm{b})} = \overline{\mathrm{P}}_{(\mathrm{c})} = \overline{\mathrm{P}}_{(\mathrm{d})}$; an extension of the global resonance condition of Ma and Zhang [50–53].

2.2.2 *Step 2: Minimising power consumption requires the absence of negative power*

We then apply this logic to the case of actuator loads in inelastic, $G^{\pm}(x)$, and elastic, $F^{\pm}(x)$, versions of the same system (Eq. 7). We first observe, that, irrespective of elasticity, $F_s(x)$, both versions represent an identical net power—metric (**a**), the loop area. Physically, this is because elastic forces are energy-conserving; and geometrically, because $F_s(x)$ adds or subtracts from $F^{+}(x)$ and $F^{-}(x)$ equally (see Fig. 3C, D). Thus, we can use elasticity to alter.

The actuator power consumption—metrics (**b**)–(**d**), in the elastic system—while keeping the net power, (**a**), constant. Given that metrics (**b**)–(**d**) can only ever be greater than or equal to the constant value of (**a**), the minimum possible value of metrics (**b**)–(**d**) is this constant value. This minimum will necessarily be achieved when there are no additional power requirements from actuator penalties (Fig. 3A)—that is, when the work loop contains no negative power. Thus, any elasticity that ensures that negative power is absent from the elastic system work loop, $F^{\pm}(x)$, will ensure that actuator power consumption is minimised, in all metrics (**b**)–(**d**).

2.2.3 *Step 3: Elastic bounding thus minimises actuator power consumption*

Which elastic profile, $F_s(x)$, will ensure that the elastic work loop, $F^{\pm}(x)$, contains no negative power? In $F^{\pm}(x)$, negative power is generated when $F^{+}(x) < 0$, or $F^{-}(x) > 0$. We can see (Eq. 7) that elasticity, $F_s(x)$, functions as a simple additive between the inelastic and elastic work loops: $F^{\pm}(x) = G^{\pm}(x) + F_s(x)$. To ensure that the upper curve, $F^{+}(x) = G^{+}(x) + F_s(x)$, is positive everywhere, it is required that $-F_s(x) \leq G^{+}(x)$. Similarly, to ensure that the lower curve, $F^{-}(x)$ is negative everywhere, $-F_s(x) \geq G^{-}(x)$ must hold. That is, to ensure that the actuator power consumption is minimised, the elastic-bound conditions of Eq. 10 must be satisfied. Figure 3C, D illustrates this principle, with the effect of exceeding a bound indicated.

2.3 Optimality in series-elastic actuation (SEA) systems under imperfect regeneration

As an alternative to PEA, series-elastic actuation (SEA) involves linking an elastic element to the system in series with the actuator (Fig. 4), in the manner of classical base excitation [68]. The dynamics of a general nonlinear time-invariant 1DOF SEA system can be represented as:

$$D(x, \dot{x}, \ddot{x}, \ldots) = F_s(u(t) - x(t)) = F(t), \tag{11}$$

where $F(t)$ is the actuator load; $x(t)$ is the prescribed system displacement (kinematic output); $u(t)$ is the actuator displacement (kinematic input); and $F_s(\cdot)$ is the elastic profile, dependent on the relative displacement $u(t) - x(t)$. While this SEA system is a direct analogue of the PEA system studied in Sect. 2.2, there are several differences in behaviour. First, the mass and dissipation of the actuation point cannot be lumped into the general time-invariant dynamics $D(\cdot)$. This is a simplifying assumption *vis-à-vis* the behaviour of many real actuators [22–24]. Second, the case of zero elasticity ($F_s = 0$) is non-physical: load transmission is impossible. Third, for a given kinematic output, $x(t)$, the load requirement, $F(t)$, is

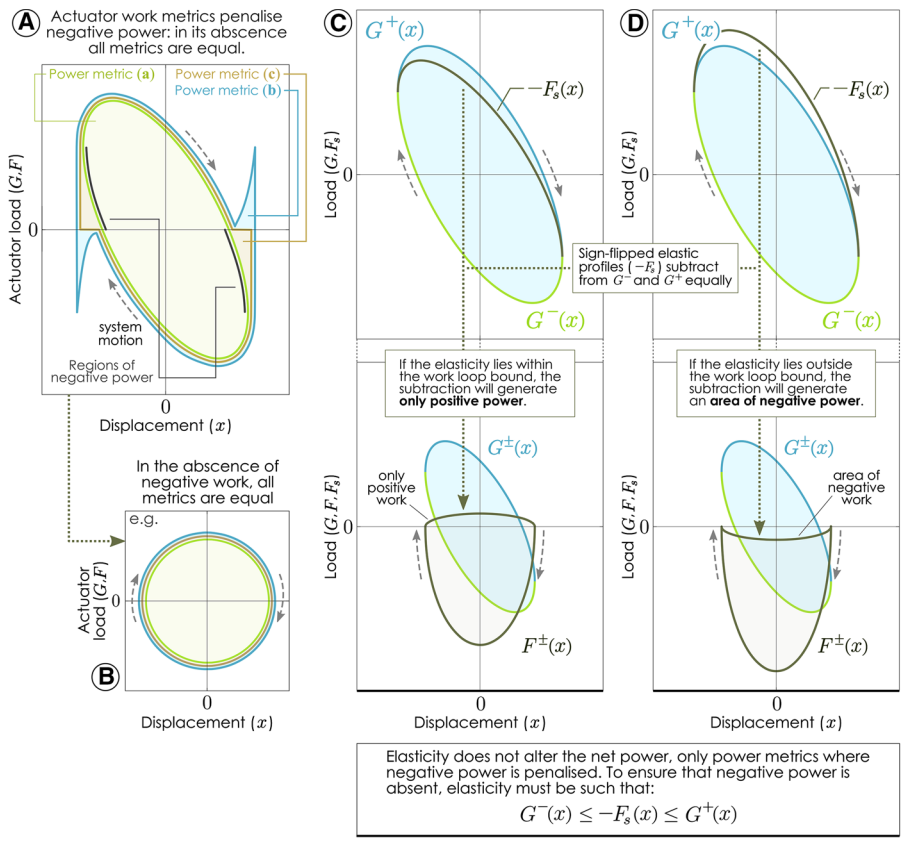

Fig. 3 Explanation of the elastic-bound conditions in PEA systems. (**A**) Work-loop interpretation of three of power metrics (a)–(c). The common feature of metrics (b) and (c) is that they penalise, in some way, regions of negative power; as such, they are particular forms of general metric (d). (**B**) In any situation, if the system work loop contains no negative power, then all metrics (a)–(d), are equivalent. (**C**) The sign-flipped elasticity, $-F_s(x)$, i.e. the elastic reaction load profile, subtracts from the original work loop bounds, $G^{\pm}(x)$, equally, but leaves the system net work, metric (a), unchanged. As such, it may be seen that, if $-F_s(x)$ lies within original work loop bounds, then the system is free from negative power, and metrics (b)–(d) take minimal values. Or, (**D**), if at any point $-F_s(x)$ exceeds one of these bounds, then an area of negative power is created, and the actuator power consumption, under metrics (b)–(d), exceeds the net power. It follows that $G^-(x) \leq -F_s(x) \leq G^+(x)$ ensures minimum actuator power consumption

independent of elasticity and dependent only on the system dynamics, $D(\cdot)$ (Eq. 11). In contrast, the actuator displacement, $u(t)$, is dependent on elasticity and links power consumption to elasticity, via $P(t) = F(t)\dot{u}(t)$. It is nevertheless possible to derive an elastic-bound optimality condition for this system, as summarised in the following four-step process:

2.3.1 *Step 1: Reformulate the system such that elasticity is additive*

Obtaining an elastic-bound condition relies on the additive properties of elasticity. To construct an additive framework for the analysis of SEA systems, we apply the inverse function of elasticity, $F_s^{-1}(\cdot)$, assuming it exists, to Eq. 11:

$$u(t) = x(t) + F_s^{-1}(F(t)). \tag{12}$$

Equation 12 then represents a displacement transmission relationship, where the inverse of elasticity, $F_s^{-1}(F(t))$, represents the compliant displacement [69]. This step places a restriction on our analysis: only invertible, i.e. monotonic, elasticities are permitted. Non-monotonic, e.g. bistable, elasticities are not. The case of zero elasticity in a PEA system is analogous to the case of zero compliance in the SEA system: $x(t)$ represents an inelastic response, and $u(t)$ an elastic one (Fig. 4A).

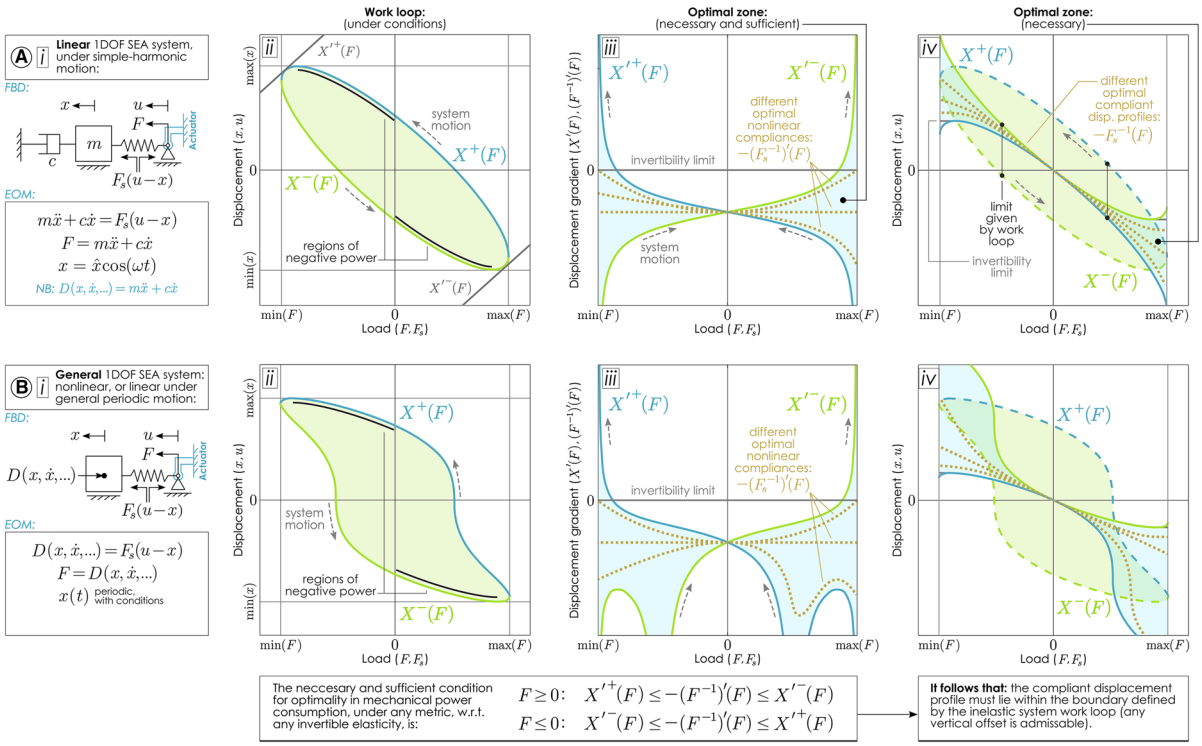

Fig. 4 Elastic-bound conditions in SEA systems. General examples in (**A**) linear systems and (**B**) nonlinear systems. In each is illustrated (**i**) system free-body diagrams (FBD) and equations of motion (EOM); (**ii**) the system work loop in the displacement–load plane; (**iii**) the elastic-bound conditions, Eq. 20, as apply to the compliance gradient; and (**iv**) the associated necessary (but not sufficient) condition on the compliant displacement profile itself, Eq. 22. Additional bounds, arising from the invertibility condition, are also illustrated

2.3.2 *Step 2: Characterise system loops in displacement–load space*

As before, the kinematic output, $x(t)$, is prescribed. It is periodic, with period T, and spans the displacement range $x(t)\in[x_1,x_2]$. By the inverse dynamics, $F(t)=D(x,\dot{x},\ddot{x},\ldots)$, (Eq. 12), it follows that $F(t)$ is also prescribed, periodic, and spans some load range $F(t)\in[F_1,F_2]$. We then visualise these periodic functions in the *rotated* displacement–load plane (F-x: abscissa F, ordinate x). In this plane, the loops traced out by $x(t)$ and $F(t)$ in x-F are still work loops (area, $\mathrm{d}F\cdot\mathrm{d}x$, is work), but $F_s^{-1}(F)$ now has an additive effect along the ordinate axis.

Following Sect. 2.2, we require that the work loop associated with the inelastic system dynamics is a closed, simple curve, no more than bivalued at any $F\in[F_1,F_2]$, and representing net power dissipation (i.e. the progression of time must represent *counter-clockwise* travel around the closed loop). More specifically, we require that the waveform $F(t)$ be composed of two half-cycles, not necessarily symmetric or in phase with $x(t)$, but each monotonic. If these conditions are fulfilled, then we can segment the inelastic work loop into upper, $X^{+}(F)$, and lower, $X^{-}(F)$, curves, associated with these separate, monotonic, half cycles in force, $F(t)$. The time windows over which this half-cycle segmentation occurs we denote $T^{\pm}$. Over each $T^{\pm}$, the force rate, $\dot{F}(t)$, takes a particular consistent sign. $T^{+}=\{t:\dot{F}(t)<0\}$ is the window associated with$X^{+}(F)$, and $T^{-}=\{t:\dot{F}(t)\geq 0\}$ is the window associated with$X^{-}(F)$. Using $T^{\pm}$, we can consistently segment a range of further variables ("Appendix A.4"):

$$\begin{aligned}&\text{velocity}:\dot{x}(t)\text{ into }\dot{X}^{\pm}(F),\\&\text{force rate}:\dot{F}(t)\text{ into }\dot{F}^{\pm}(F),\\&\text{actuator disp.}:u(t)\text{ into }U^{\pm}(F),\\&\text{actuator velocity}:\dot{u}(t)\text{ into }\dot{U}^{\pm}(F),\\&\text{actuator power}:P(t)\text{ into }P^{\pm}(F).\end{aligned}\tag{13}$$

For instance, the values of $\dot{X}^{+}(F)$ are the values of $\dot{x}(t)$ at the times $t \in T^{+}$, associated with $X^{+}(F)$. Note $\dot{X}^{\pm}(F)$ and $\dot{F}^{\pm}(F)$ are already prescribed, by $\dot{x}(t)$ and $\dot{F}(t) = dF/dt$, respectively. Using the segmentations in Eq. 13, we can also formulate Eq. 12 in the F-x plane, in a way that is directly analogous to the PEA system formulation (Eq. 7):

$$U^{\pm}(F) = X^{\pm}(F) + F_s^{-1}(F). \tag{14}$$

2.3.3 Step 3: Characterise actuator power consumption with respect to elasticity

Despite the fact that area ($dx \cdot dF$ and $dF \cdot dx$) in both F-x and x-F spaces represents mechanical work, the condition for negative power in the SEA system—loops $X^{\pm}(F)$ and $U^{\pm}(F)$—is not as simple as in the PEA system. Returning to a time-based formulation of mechanical power, $P(t) = \dot{u}(t)F(t)$, we observe the derivative relation:

$$P(t) = \frac{d}{dt}(u(t)) \cdot F(t) = \frac{d}{dF}(u(t)) \cdot \dot{F}(t) \cdot F(t), \tag{15}$$

when $u(t)$ and $F(t)$ are differentiable. This relation transforms to the x-F space as:

$$P^{\pm}(F) = U'^{\pm}(F) \cdot \dot{F}^{\pm}(F) \cdot F. \tag{16}$$

This expression for power consists of a multiplication of three terms: F, $\dot{F}$, and $U' = dU/dF = du/dF$. Differentiating Eq. 14 with respect to F, we obtain $U'^{\pm}(F)$ as:

$$U'^{\pm}(F) = X'^{\pm}(F) + \left(F_s^{-1}\right)'(F). \tag{17}$$

$\left(F_s^{-1}\right)'(F)$ is the derivative of the inverse of the elastic load profile: the nonlinear compliance or flexibility (structural mechanics) or the reciprocal of the quasi-stiffness (biomechanics) [70]. $X'^{\pm}(F)$ is the derivative of $X^{\pm}(F)$ with respect to F. $X'^{\pm}(F)$ may be computed directly from $X^{\pm}(F)$, or via:

$$X'^{\pm}(F) = \frac{\dot{X}^{\pm}(F)}{\dot{F}^{\pm}(F)}. \tag{18}$$

Equations 17 and 18 define $P^{\pm}(F)$ from Eq. 16, with the only remaining unknown being the system elasticity, expressed as $\left(F_s^{-1}\right)'(F)$.

2.3.4 Step 4. Derive elastic-bound conditions

To obtain an elastic-bound condition for SEA systems, we must answer several questions. First, does elasticity, $F_s(\cdot)$, alter the net power, $\overline{P}_{(a)}$ (Eqs. 1, 8)? It does not: physically, elasticity is conservative, and formally, integrating Eq. 18 over the work loop causes $\left(F_s^{-1}\right)'(F)$ to vanish. Second, what is the relationship between power consumption metrics (**b**)–(**d**) and the net power, metric (**a**)? We may confirm again that metrics (**b**)–(**d**) are always greater than or equal to metric (**a**) and that the absence of negative work, $P(t) \geq 0$, $\forall t$, is the sole condition for these metrics to all be equal ("Appendix A.4"). Finally, does the elasticity alter metrics (**b**)–(**d**)? In general, it does. It follows then that any elasticity which ensures that negative power is absent from the system necessarily minimises metrics (**b**)–(**d**).

What, then, are the conditions on elasticity to ensure that negative power is absent? By Eqs. 15, 16 negative power, $P^{\pm}(F) < 0$, occurs when the signs of the force (F), force rate ($\dot{F}$), and gradient of the resultant work loop (U'), all multiply to be negative (Fig. 4). Note that this condition may be confirmed by rotating the loop back to displacement–load space (u-F) and observing where $P = F\dot{u}$ changes sign. To ensure only positive power is present, $P^{\pm}(F) \geq 0$, $\forall F \in [F_1, F_2]$, we substitute Eq. 17 into Eq. 16 and obtain:

$$-\left(F_s^{-1}\right)'(F) \cdot \dot{F}^{\pm}(F) \cdot F \leq X'^{\pm}(F) \cdot \dot{F}^{\pm}(F) \cdot F, \forall F \in [F_1, F_2]. \tag{19}$$

Accounting for all possible combinations of signs for F and $\dot{F}$ ("Appendix A.4"), we obtain a set of conditions on $\left(F_s^{-1}\right)'(F)$. These are the SEA elastic-bound conditions:

$$\begin{aligned} &\text{for} \quad F_1 \leq F \leq 0 : X'^{-}(F) \leq -\left(F_s^{-1}\right)'(F) \leq X'^{+}(F); \\ &\text{for} \quad 0 \leq F \leq F_2 : X'^{+}(F) \leq -\left(F_s^{-1}\right)'(F) \leq X'^{-}(F); \end{aligned} \tag{20}$$

which are sufficient for energetic optimality, under imperfect energy regeneration, metrics (**b**)–(**d**), and under the system conditions that have been outlined (invertible elasticity, relevant curve conditions). This concludes the four-step process for formulating the

elastic-bound condition in this SEA system—a full proof, as well as a derivation of $X'^{\pm}(x)$ in a specific case, is presented in "Appendix (A.2, A.4)". In intuitive terms: negative power is generated when U' reverses direction within a half-cycle, as this represents a reversal in $\dot{u}$ ($P = F\dot{u}$). To eliminate this negative power, we require that the gradient of the compliance, $\left(F_s^{-1}\right)'$, is bounded by X', because these three gradient terms show an additive relationship, $U' = X' + \left(F_s^{-1}\right)'$. Figure 4 shows a visualisation of these elastic-bound conditions, in general linear and nonlinear SEA systems, alongside several key notes, as follows:

Note (**i**) The requirement for invertible elasticity necessitates that the elasticity be either always-stable, $\left(F_s^{-1}\right)'(F) \geq 0, \quad \forall F \in [F_1, F_2]$, or always-unstable, $\left(F_s^{-1}\right)'(F) \leq 0, \ \forall F \in [F_1, F_2]$, with no more than a single equilibrium (Fig. 4).

Note (**ii**) Equation 20, as stated, is sufficient but not necessary for optimality. Equation 20 becomes necessary if the inelastic system itself, expressed as $X'^{\pm}(F)$, satisfies a set of further conditions:

$$\begin{aligned} &X'^{+}(F) \geq X'^{-}(F), \forall F \in [F_1, 0], \\ &X'^{-}(F) \geq X'^{+}(F), \forall F \in [0, F_2], \\ &\quad \text{and,} \quad X'^{+}(0) = X'^{-}(0). \end{aligned} \tag{21}$$

That is, if Eq. 20 is satisfied, the actuator power requirement, $P(t)$, contains no negative power. In a given system, it is not immediately guaranteed that any elasticity exists satisfying Eq. 20: the condition on the system ($X'^{\pm}$) for such an elasticity to exist is Eq. 21. Note that, in systems not satisfying Eq. 21, it is still possible to optimise power consumption, but the optimal state will still contain regions of negative power, and Eq. 20 will not be satisfied. This accessibility of optimal states without negative power is a topic that warrants further investigation.

Note (**iii**) Equation 20 defines a continuous range of optimal compliance profiles. These profiles show a common feature: Eq. 20 functions as an equality condition at the point of zero load ($F = 0$), implying that the compliance at $F = 0$, $\left(F_s^{-1}\right)'(0)$, must take the value common to $-X'^{\pm}(0)$ (Eq. 21), to ensure energetic optimality via the absence of negative work.

Note (**iv**) Equation 20 is a condition on the compliance of the elastic element, $\left(F_s^{-1}\right)'(F)$: the gradient of the compliant displacement profile, not the displacement profile itself. Any offset is permissible, i.e. any C in $F_s^{-1}(F) = \int \left(F_s^{-1}\right)'(F) dF + C$, though such an offset is not useful: it merely represents a static offset in the actuator displacement, $u(t)$, with the actuator displacement about the system equilibrium, $u(t) - F_s^{-1}(0)$, remaining unaltered.

Note (**v**) Integrating Eq. 20 yields a condition on the compliant displacement profile itself, $F_s^{-1}(F)$, giving its maximum range:

$$\begin{aligned} X^{+}(F) - X^{+}(0) \leq\ &- F_s^{-1}(F) - F_s^{-1}(0) \leq X^{-}(F) \\ &- X^{-}(0), \end{aligned} \tag{22}$$

where $X^{\pm}(0)$ and $F_s^{-1}(0)$ account for the fact that $F_s^{-1}(0)$ can equal any constant (note **iv**). Figure 4 illustrates this condition. Equation 22 is necessary, but not sufficient, for optimality: the gradient condition, Eq. 20, must still be satisfied within these bounds.

2.4 Additional objectives and constraints: variant and invariant metrics

Our objective thus far has been to minimise actuator mechanical power consumption, but many other objective and constraint metrics may be relevant to the actuator at hand (peak power, duty cycle, etc.). Indeed, the non-uniqueness of the optimal solutions in Sects. 2.2, 2.3 naturally leads to a consideration of additional metrics: one may choose from this pool of non-unique solutions, or search space, to achieve other objectives, possibly at no further cost. Different metrics are relevant to different actuators, but broadly, we can classify them all as either variant or invariant—referring to whether or not they vary over the space of non-unique elasticities given by the system's elastic-bound conditions. With a few subtleties, the definition of the invariant metrics implies that optimality in these metrics comes simultaneously with optimality in mechanical power. Variant metrics, on the other hand, vary across the non-unique solution pool, and thus are more complex to optimise.

So, which metrics are invariant? In the SEA system, the actuator load profile, $F(t)$, is completely independent of elasticity—though note that this independence

does rest on our simplification of actuation point dynamics (inertialess actuation point, etc., see Sect. 2.3). Any functional solely of $F(t)$ is thus an invariant metric in SEA systems: for instance, peak load, $\max|F|$, duty cycle, and electrical resistive losses, measured via the force-squared metric [30, 31, 41]:

$$\overline{\mathrm{P}}_{F^2} \propto \frac{1}{T}\int_0^T F(t)^2 dt. \tag{23}$$

Also invariant are several isometric muscular power consumption metrics, measured via a range of force-based metrics, including $\overline{\mathrm{P}}_{F^2}$ and also [39, 40, 59, 71]:

$$\begin{aligned} &\overline{\mathrm{P}}_{|F|} \propto \frac{1}{T}\int_0^T |F(t)| dt, \overline{\mathrm{P}}_{|\dot{F}|} \propto \frac{1}{T}\int_0^T \left|\dot{F}(t)\right| dt, \\ &\overline{\mathrm{P}}_{\dot{F}^2} \propto \frac{1}{T}\int_0^T \dot{F}(t)^2 dt. \end{aligned} \tag{24}$$

Given $F(t)$'s independence in SEA systems, optimality (i.e. neutrality) in all these metrics comes guaranteed.

Other potentially relevant metrics are, however, variant: metrics including the peak power, $\max|P|$, and any functional of the actuator displacement, $u(t)$. In general, optimising or constraining these metrics requires additional analysis. Extensions to our analytical framework can provide certain additional results—for instance, we note that constraints on the actuator displacement could be translated back to constraints on the elasticity, via Eq. 17. Otherwise, in the general case, convex optimisation [22–24] may be able to optimise complex variant metrics, though characterising any non-uniqueness in the optimum may be difficult.

In PEA systems, $x(t)$ is prescribed and thus completely independent of elasticity. Any functional solely of $x(t)$ is an invariant metric: associated constraints or objectives can be trivially included in the initial prescription. Functionals of force, $F(t)$, are generally variant metrics, requiring additional optimisation, convex, or otherwise. We note, for instance, that the PEA midline elasticity, $-F(x) = -G_{\mathrm{mid}}(x)$, is a non-unique minimum for several variant metrics, such as the peak load, $\max|F|$. But there is one key exception to the variance of force-based metrics. In PEA systems, the absolute force metric, $\overline{\mathrm{P}}_{|F|}$, is invariant over the space of elastic-bound solutions, provided that the prescribed displacement, $x(t)$, shows the symmetry $x(t) = x(T - t), \forall t$ (i.e. is composed of two symmetric half-cycles). A proof is given in "Appendix (A.5)". This symmetry condition is satisfied for many common waveforms: sine waves, triangle waves, square waves, etc., and for these waveforms, all of the elastic bound solutions are equally optimal in $\overline{\mathrm{P}}_{|F|}$. This conditional invariance of $\overline{\mathrm{P}}_{|F|}$ implies that PEA systems may be better suited for optimising biological systems, for which $\overline{\mathrm{P}}_{|F|}$ is relevant [72], than to optimising electromechanical ones, for which $\overline{\mathrm{P}}_{F^2}$ is more relevant.

3 Systems-design applications

3.1 Exploring the elastic-bound solution space

The elastic-bound conditions of Sects. 2.2, 2.3 define a space of non-unique optimal nonlinear elasticities, all minimising the mechanical power consumption of an actuator with imperfect energy regeneration. This space of elasticities may encompass various forms of elastic behaviour: e.g. linear, strain-hardening, strain-softening, bistable, freeplay, and others. The choice of elasticity, and elastic behaviour, is a design tool: it allows additional optimisation objectives to be pursued (Sect. 2.4); allows actuator input waveforms to be tuned according to the desired actuation characteristics; and allows different forms of behaviour to be designed into the system, all while retaining overall energetic optimality. Multiple approaches to making this choice are available. In Sect. 2.4, we laid a theoretical groundwork for the study of additional objectives, through the classification of variant and invariant metrics. If particular quantitative design objectives are pursed, then convex-optimisation techniques [22–24] can be applied, alongside invariance principles, to locate optimal states associated with these objectives. Alternatively, particular forms of optimal elasticity (e.g. bistable, freeplay) can be studied generally, and their effect on the system and actuator behaviour can be characterised. The latter is the approach that we present—and we go further to

explore specific applications and actuators that are well-suited to particular forms of elasticity.

We consider the trade-offs between four key aspects of system and actuator behaviour. (**i**) Peak actuator load and power. These are general metrics of capability, rather than efficiency. (**ii**) Actuator duty cycle: the cycle-normalised time window over which the actuator load is nonzero. Several actuator types, including solenoids and shape memory alloys, operate at greater efficiency under low duty-cycle operation [35, 73–75], often for temperature-related reasons. In general, there is a trade-off between peak load/power and duty cycle, the priority of the two resting on the actuator in question. (**iii**) Directionality of actuator load: a range of actuators (solenoids, muscles, etc.) are capable of only unidirectional load outputs [72–75]. Generating a bidirectional load profile requires actuator duplication, with attendant control complexity. By selecting an appropriate nonlinear elasticity, we may be able to reduce the load requirement to a unidirectional profile, eliminating the need for actuator duplication. (**iv**) The system behaviour under off-nominal loading conditions. While each combination of optimal elasticity and input load waveform will recreate the prescribed nominal output, the behaviour of the system at off-nominal conditions (e.g. quasistatic, free-response, differing frequency, etc.) will differ sharply. Over the following two sections, we detail some of the choices of elasticity that can be made, and their implications for these aspects of system and actuator behaviour.

3.2 PEA systems-design applications

In PEA systems, the actuator load waveform, $F(t)$, is not invariant. This has the advantage of allowing particular load waveform properties to be designed into the system. In addition, our PEA analysis framework permits non-invertible elasticities (e.g. bistable elasticities), allowing significant control over the system equilibria and quasistatic behaviour. Figure 5 describes several forms of optimal elasticity in a general PEA system, and their implications.

3.2.1 Freeplay elasticities

Freeplay elasticities are characterised by a region of zero elastic force—the freeplay region—often located around a rest state. For instance, the elastic force profile:

$$F_s(x) = \begin{cases} k(x+\delta) & x \le -\delta, \\ 0 & -\delta \le x \le \delta, \\ k(x-\delta) & x \ge \delta, \end{cases} \qquad \delta \ge 0 \tag{25}$$

Freeplay elasticities commonly arise from backlash (i.e. clearance and tolerance) effects in rigid mechanisms such as gear trains [76] and are typically unintentional and undesired. According to our analysis, however, freeplay elasticities can still be energetically optimal: a range of different freeplay elasticities satisfy the PEA elastic-bound conditions. For instance, defining displacements $l^{\pm}$ such that $G^{+}(l^{+}) = 0$ and $G^{-}(l^{-}) = 0$, we find that any freeplay with $0 \le \delta \le \min\{-l^{+}, l^{-}\}$, can be optimal, with the correct$k$. This optimal freeplay stiffness (k) is given by substituting Eq. 25 into Eq. 10: it differs from the optimal linear stiffness, and is typically greater. While the use of freeplay elasticities leads to a load requirement (Fig. 5Aiv) that shows greater peak load and peak power requirement than is the case when the system contains no freeplay (e.g. under perfect linear elasticity, also illustrated), our approach nevertheless allows the construction of a system in which the overall power consumption is optimal. Note also that the existence of this broad class of optimal freeplay elasticities highlights a difference between our method, and existing convex optimisation methods [22–24]: our method is able to completely describe this set of optimal freeplay elasticities (of the form of Eq. 25). Existing convex-optimisation approaches are limited to single-point convergence [22–24], and cannot describe a non-unique solution space in the same way.

There are also cogent reasons to consider the intentional use of freeplay elasticities in PEA systems. For instance, consider a system designed for two modes of operation—a high-frequency mode and a quasistatic mode. Such a system could represent several forms of biomimetic propulsion and/or flow control, e.g.: (**i**) a legged robot [21, 58] designed both for running and for slow, careful, walking; (**ii**) an aquatic robot [78, 79] designed for both rapid and slow swimming; or (**iii**) an active gurney flap in an aerofoil or hydrofoil [80], designed for both oscillatory flow control and slow flight control. Applying the elastic-bound conditions to the high-frequency mode, we

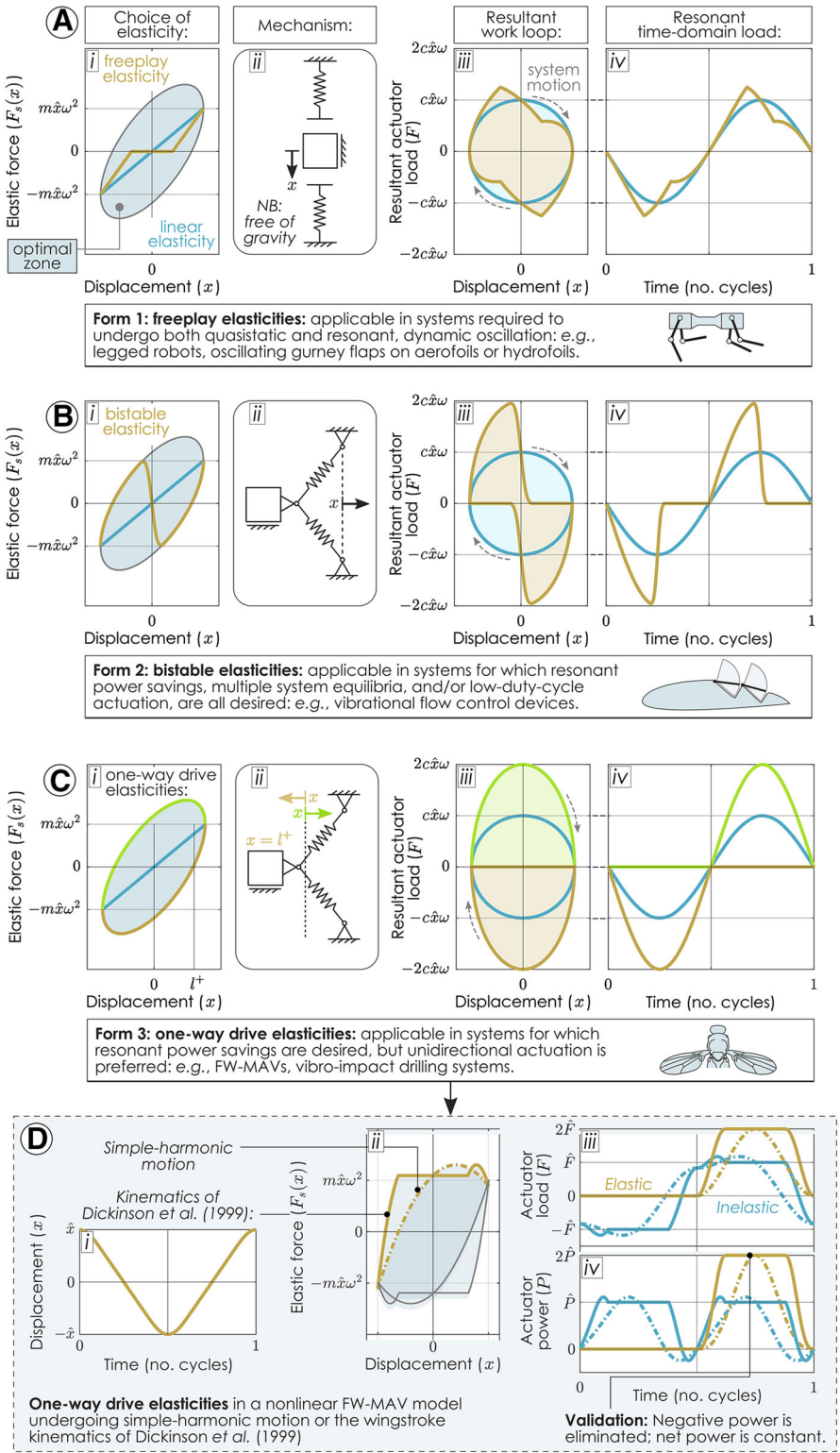

Fig. 5 Systems-design applications of optimal nonlinear elasticity in PEA systems. Three forms of optimal nonlinear elasticity are illustrated: (**A**) freeplay-nonlinear elasticities; (**B**) bistable elasticities; (**C**) the one-way drive elasticities. For each form is shown: (**i**) the nonlinear elastic load profile, within the optimal zone, and compared to a resonant linear elasticity; (**ii**) a two-dimensional mechanism approximating the nonlinear elasticity via geometric nonlinearity; (**iii**) the resultant work loops, for both the nonlinear and linear elasticity; (**iv**) the resultant time-domain actuator loads. (**C**) An FW-MAV application: one-way drive elasticities for a nonlinear FW-MAV with quadratic damping ($G = m\ddot{x} + c\dot{x}|\dot{x}|$), undergoing either simple-harmonic motion or the insect wingbeat kinematics identified by Dickinson et al. [77]. (**i**) Wingbeat kinematics; (**ii**) one-way drive elasticities; (**iii**) the elastic (resultant) and inelastic time-domain actuator load profiles, scaling $\widehat{F} = c\hat{x}^2\omega^2$; (**iv**) elastic and inelastic time-domain actuator power profiles, scaling $\widehat{P} = c\hat{x}^3\omega^3$, confirming energetic optimality: these elasticities eliminate negative power, while maintaining constant net power

obtain a range of elasticities minimising the mechanical power consumption of this high-frequency state. However, some of these elasticities (e.g. a resonant linear elasticity) introduce a problem: during the quasistatic mode the actuator must actively apply load against the elasticity. A freeplay elasticity (e.g. Figure 5Ai) provides one solution to this problem: over the freeplay region, a certain displacement range in x, the quasistatic mode of operation has zero load elastic load requirement. A freeplay elasticity thus allows the efficiency and performance of the quasistatic mode of operation to be increased, at no cost to the mechanical power consumption of the high-frequency mode of operation. Manufacturing such elasticities presents no practical problem: contact mechanisms can generate freeplay elasticities of arbitrary width (Fig. 5Aii).

3.2.2 *Bistable elasticities*

Bistable elasticities consist of an unstable equilibrium bracketed by stable equilibria. The existence of bistable (and multistable) elasticities satisfying the PEA elastic-bound conditions thus allows a range of different system equilibria to be designed into the system at no overall energetic cost. For instance, elasticities with stable equilibria at high displacement (Fig. 5Bi) may be useful for systems designed to oscillate outwards from a retracted equilibrium—for instance, active gurney flaps [80], in which an equilibrium located near an extremum of the oscillatory displacement range may represent a streamlined aerofoil profile. Bistable elasticities also allow a degree of control over the actuator duty cycle: a bistable elasticity tuned to lie along the boundary of the inelastic system work loop, i.e. tuned to both the inertia and the dissipation of the system, can reduce the actuator duty cycle down to 50% (Fig. 5Biv) or even below.[1] This reduction in duty cycle could be used to optimise the behaviour of solenoid actuators, as noted in Sect. 3.1. For example, consider the family of elasticities:

$$F_s(x) = \begin{cases} -G^-(x) & x \le -\delta, \\ -G^+(\delta)\dfrac{x}{\delta} & -\delta \le x \le \delta, \\ -G^+(x) & x \ge \delta, \end{cases} \tag{26}$$

controlled by the parameter δ. For $0 < \delta \le \max(x)$, in a system showing symmetry $x(t) = x(T - t), \forall t$, this elasticity satisfies the elastic-bound conditions (Sect. 2.2). For $0 < \delta < l^+$, where l^+ are such that $G^+(l^+) = 0$, this elasticity is bistable; for $\delta = l^+$, this elasticity is a freeplay strain-hardening elasticity; for $l^+ < \delta < \max(x)$, the elasticity is strain hardening; and for $\delta = \max(x)$ the elasticity is linear. In the bistable regime, $0 < \delta < l^+$, the duty cycle of the actuator load requirement waveform reaches 50% in the limit $\delta \to 0$. While this limit is not practically achievable, operating near this limit (Fig. 5Aii) leads to similarly low duty cycles. This allows the construction of energetically optimal resonant drive systems using actuators which are only capable of providing low duty-cycle load waveforms. In manufacturing terms, bistable elasticities can be generated from monotonic (even, linear) elasticities via a range of bistable mechanisms [81]—for instance, the mechanism in Fig. 5Bii.

3.2.3 *The one-way drive elasticities*

In any PEA system satisfying our analysis conditions (Sect. 2.2), a pair of unique elasticities ($F_{s,1}$ and $F_{s,2}$) necessarily exist:

$$\begin{aligned} F_{s,1}(x) &= -G^+(x), \\ F_{s,2}(x) &= -G^-(x). \end{aligned} \tag{27}$$

These elasticities (Fig. 5Ci) represent the upper and lower boundaries of the sign-flipped work loop, $-G^{\pm}(x)$, the boundaries of the elastic-bound conditions (Eq. 10). Recalling that $F^{\pm}(x) = G^{\pm}(x) + F_s(x)$ (Eq. 7), we observe that these elasticities leave one boundary of the resultant work loop at a state of zero load:

$$\begin{aligned} F_{s,1}(x) = -G^+(x) \Rightarrow F^+(x) = 0, \quad F^-(x) = -2G_{\text{arc}}(x), \\ F_{s,2}(x) = -G^-(x) \Rightarrow F^-(x) = 0, \quad F^+(x) = 2G_{\text{arc}}(x). \end{aligned} \tag{28}$$

As a result, the actuator load requirement is *unidirectional* (Fig. 5Civ). For this reason, we term $F_{s,1}(x)$ and $F_{s,2}(x)$ the one-way drive elasticities. They

[1] The limit is a state of zero load over 50% of the *work loop* (Fig. 5Aii). If different quarter-cycles of the work loop are kinematically faster than others, then the limit of the time-domain duty cycle can be $< 50\%$.

are optimal, according to the elastic-bound conditions, and, at a cost of doubling the peak load and power, reduce the actuator duty cycle down to 50% or lower.[2] Physically, these elasticities optimally recreate one half-cycle of the oscillatory motion, via stored energy from the other half cycle.

The implications of the one-way drive elasticities are extensive. They allow a single low duty-cycle unidirectional actuator (e.g. a solenoid or combustion cylinder) to generate energetically optimal resonant oscillations. This is in contrast to conventional resonant forced-oscillation systems, which are typically subjected to bidirectional actuation, as a necessary condition of linear resonance. The possibility of energetically optimal unidirectional actuation significantly simplifies actuation requirements and allows new classes of actuator to be used, without duplication. A particularly relevant application is in flapping-wing micro-air-vehicles (FW-MAVs), which stand to benefit significantly from a reduction in actuation system mass and/or complexity. Figure 5D illustrates an FW-MAV application in more detail: we study a quadratically damped nonlinear system ($G = m\ddot{x} + c\dot{x}|\dot{x}|$, cf. "Appendix, A.1") with $c/m = 1.2$, undergoing either normalised simple-harmonic motion, or the normalised wingbeat kinematics identified by Dickinson et al. [77] as a model of insect flight. In each of these cases, we construct and validate an appropriate one-way drive elasticity: computing the load and power requirement waveforms under inelastic and elastic conditions, we confirm that introducing the appropriate one-way drive elasticity into the system reduces the load requirement to unidirectionality and eliminates negative power in the system, while maintaining constant net power. These elasticities are thereby optimal, according to the analysis of Sect. 2.2. In manufacturing terms, while the details of the elastic profile may be complex, the basic form of these one-way drive elasticities could be effectively represented by bistable elasticities operating to one side of an unstable equilibrium (Fig. 5Cii)—a method for generating these nonlinear elasticities via geometric nonlinearity, rather than material nonlinearity.

3.2.4 Special case: dissipation-dominated systems

An interesting behaviour arises in dissipation-dominated systems (Fig. 5B), with zero effective inertia and initial elasticity, i.e. $D(x, \dot{x}, \ddot{x}, \ldots) \approx D(\dot{x})$, with $D(0) \approx 0$. In such systems, the elastic-bound conditions describe a space of energetically neutral elasticities. With zero effective inertia, elasticity cannot reduce the actuator mechanical power consumption, but it can hold it constant, and at the same time, alter other system properties. For instance, optimal bistable elasticities can be constructed in order to alter the system equilibria and their stability, and reduce actuator duty cycle (Sect. 3.2.2). One-way drive elasticities can be constructed to reduce the actuator load requirement to unidirectionality, and to reduce actuator duty cycle (Sect. 3.2.3). Simple (e.g. piecewise-linear) optimal freeplay elasticities reduce to the trivial case of zero elasticity (Sect. 3,2,1), but more complex optimal freeplay and/or contact-based elasticities can be constructed. For instance, consider a destabilising elasticity with a single stable equilibrium and two unstable equilibria (Fig. 6A): using this nonlinear elasticity, we can construct a high-stability equilibrium in a dissipation-dominated system, while maintaining energetic neutrality. Energetically neutral elasticities such as these may have applications in low Reynolds number locomotion systems [82, 83]. They may also provide insight into the role of elastic structures in biological instances of such systems [84]: the evolutionary motivation for these structures may be the synchronisation of muscular load capability with propulsion load requirements, alongside or instead of any overall energy savings.

3.3 SEA systems-design applications

Comparing SEA to PEA systems, in the context of the elastic-bound conditions, we note the following advantages and disadvantages. *Advantage*: in SEA systems, the actuator load requirement is independent of elasticity. The elastic-bound solution space can be explored while retaining invariance in, e.g. electrical resistive losses, and peak load requirement. *Disadvantage* (**i**): as a corollary, elasticity cannot be used to alter the load requirement waveform. Low duty-cycle

[2] 6 If the kinematic waveform, $x(t)$, is composed of two symmetric half-cycles, *i.e.*, $x(t) = x(T - t), \forall t$, then both one-way drive elasticities will generate load waveforms of duty cycle 50% (Fig. 5Ciii). If this is not the case, then one will generate a waveform of duty cycle $< 50\%$, and the other, a waveform of duty cycle $> 50\%$.

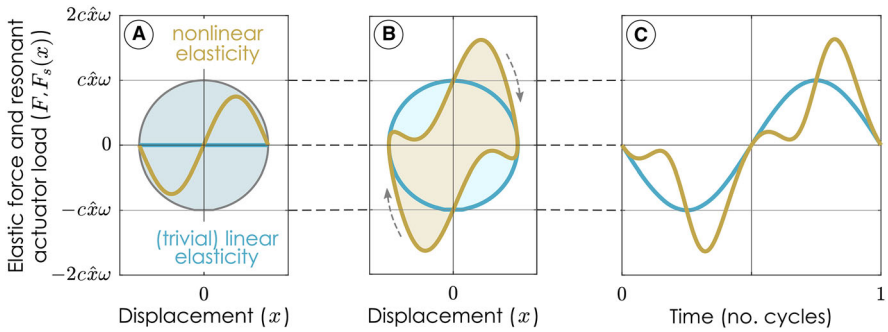

Fig. 6 The special case of dissipation-dominated PEA systems. In such systems, e.g. low-Reynolds number locomotion systems, alteration of system properties (duty cycle, equilibria, etc.) can be achieved at a state of energetic neutrality. (**A**) An example energetically neutral nonlinear elastic load profile, creating a stable equilibrium within the system, compared with the trivial resonant linear elasticity. (**B**) The resultant work loops. (**C**) The resultant time-domain actuator loads

or one-way drive systems cannot be constructed. *Disadvantage* (**ii**): our analysis does not permit non-invertible, e.g. bistable, elastic profiles in SEA systems. *Disadvantage* (**iii**): the elasticity at the system's equilibrium point is prescribed (Eq. 20). Overall, compared to PEA systems, the range of optimal elastic behaviour available in SEA systems is more limited—but there is one available form of behaviour worth noting.

3.3.1 The dwell-time elasticities

As in PEA systems, elasticities in SEA systems that lie along the boundary of the optimal region (Eq. 20) show special properties. These properties manifest not in load, $F(t)$, which is invariant, but in actuator displacement, $u(t)$. For instance, consider the elasticities given by:

$$\begin{aligned}\left(F_s^{-1}\right)'(F) &= -X'^{+}(F),\ e.g.\ F_s^{-1}(F) = -X^{+}(F),\\ \left(F_s^{-1}\right)'(F) &= -X'^{-}(F),\ e.g.\ F_s^{-1}(F) = -X^{-}(F),\end{aligned} \tag{29}$$

as shown in Fig. 6. These elasticities ensure that one side of the actuator work loop, $U^{\pm}(F)$, lies at a state of *zero displacement*. Recalling that $U^{\pm}(F) = X^{\pm}(F) + F_s^{-1}(F)$ (Eq. 14):

$$\begin{aligned}F_s^{-1}(F) = -X^{+}(F) &\Rightarrow U^{+}(F) = 0,\\ F_s^{-1}(F) = -X^{-}(F) &\Rightarrow U^{-}(F) = 0.\end{aligned} \tag{30}$$

In other words, for approximately a half-cycle, the actuation point, $u(t)$, is motionless. These elasticities are the analogue of the one-way drive elasticities in the PEA system: they generate a low duty-cycle profile in actuator velocity, $\dot{u}(t)$, rather than in the actuator load, $F(t)$. This dwell-time property may be of utility: for instance, it allows prolonged contact between the moving actuation point, $u(t)$, and another structure fixed in the external reference frame—potentially facilitating the transmission of information, energy, fuel, or material to the system each cycle. This property can be replicated in dissipation-dominated systems—except, at a state of energetic neutrality rather than optimality—and it retains the SEA advantage of invariant electrical resistive losses ($\overline{\mathrm{P}}_{F^2}$). Overall, SEA systems show lesser variety in the types of optimal elasticity than PEA systems, but maintain invariance in a wider range of metrics.

4 Implications and discussion

4.1 Is this behaviour resonant?

We derived the elastic-bound conditions (Sects. 2) as a description of the solutions to a particular optimisation problem: mechanical power minimisation under imperfect energy regeneration. In doing so, we also describe a certain nonlinear resonant phenomenon. By construction, the optimal elasticities given by the elastic-bound conditions absorb all power requirements associated with the system inertia. The resulting overall actuator power consumption is equal to the net power (Eq. 1) and thus is dependent only on the system dissipation. In this sense, the resulting actuated states are energetically equivalent to linear

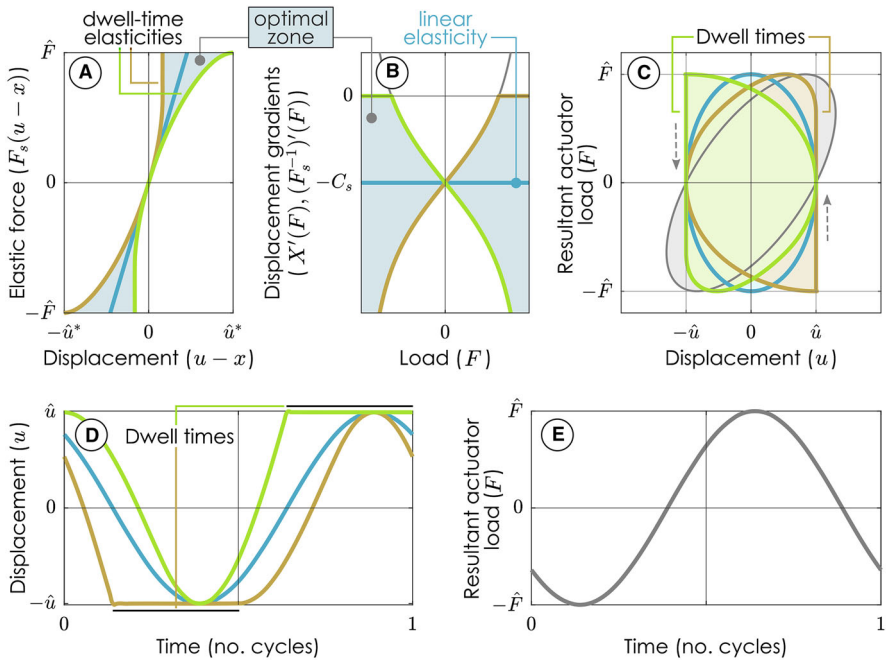

Fig. 7 The dwell-time elasticities in an SEA system. These elasticities generate a prolonged period in which the actuation point,$u(t)$, is motionless. Applications include systems requiring a contact-based transfer (e.g. of material, energy) through the vibrating system (e.g. in a manufacturing process). (**A**) The two dwell-time elastic profiles within the optimal zone, and compared to a resonant linear elasticity. (**B**) These profiles in gradient space, $X'(F)$. (**C**) The resultant actuator work loops, indicating the dwell times. (**D**) The resultant time-domain actuator displacement profiles, indicating the dwell times. (**E**) The resultant time-domain actuator load profile, which is invariant with respect to elasticity (Sect. 2.4). Note the scaling parameters: $\hat{u} = \hat{x}c/\sqrt{m^2\omega^2 + c^2}$; $\hat{u}^* = \hat{x}(m\omega + c)/\sqrt{m^2\omega^2 + c^2}$; $\hat{F} = \omega\hat{x}\sqrt{m^2\omega^2 + c^2}$ and $C_s = \left(F_S^{-1}\right)'(0) = m/(m^2\omega^2 + c^2)$ (cf. "Appendix A.2")

resonant states: they represent an energetic generalisation of linear resonance. Nonlinear resonance is a complex phenomenon and is characterised in different ways in different contexts: in terms of global resonance [50–53], coherence resonance [85, 86], the jump phenomenon [87, 88], or resonant wave interaction [89]. Our energetic resonance is equivalent to the global resonance of Ma and Zhang [50–53]. The absence of negative power ($P(t) > 0, \forall t$), i.e. a state of ideal energy transfer through the system, is both the core condition for global resonance [50–53] and the core condition for power optimality under imperfect energy regeneration. In an analogy with classical transfer-function analysis, these global resonant/energetically optimal states can be seen as the concurrent maxima of a family of energy-based nonlinear transfer ratios: the power metric ratios $\overline{\mathrm{P}}_{(\mathrm{a})}/\overline{\mathrm{P}}_{(i)}$, $i \in \{\mathrm{b}, \mathrm{c}, \mathrm{d}\}$, and also the input–output power transfer ratios (H):

$$\text{PEA: } H = \frac{\int_0^T |G\dot{x}|dt}{\int_0^T |F\dot{x}|dt}, \quad \text{SEA: } H = \frac{\int_0^T |F\dot{x}|dt}{\int_0^T |F\dot{u}|dt}. \tag{31}$$

These transfer ratios represent the ratio of system output power (PEA: $G\dot{x}$, SEA: $F\dot{x}$) to system input power (PEA: $F\dot{x}$, SEA: $F\dot{u}$), in absolute terms. These transfer ratios are extensions of power-, energy- and work-based transfer functions in linear systems, as used, for example, in vibroacoustics [90, 91], seismic base excitation [92, 93], and energy harvesting [94]. In this way, we observe a fundamental link between the elastic-bound conditions, the energetic properties of linear resonance, and nonlinear global resonance.

4.2 Implications for optimal design of biomimetic propulsion systems

The elastic-bound conditions describe a set of energetically optimal nonlinear elasticities that are practically relevant: they represent states of optimality in

power-metrics ($\overline{P}_{(b)}$, $\overline{P}_{(c)}$, $\overline{P}_{(d)}$), that do not assume idealised energy recovery. Small-scale biomimetic propulsion systems, such as FW-MAVs and micro-swimmers, are an application area where these considerations are pertinent, as these systems typically utilise very simple power electronics, or even, non-electrical actuators, e.g. external acoustic forcing [82]. The elastic-bound conditions both describe a set of realistic energetically optimal nonlinear elasticities for these systems and lead to methods for simultaneously controlling a range of different system properties. In PEA architectures, we demonstrated control of the system quasistatic response; control of system equilibria stability and location; and a reduction in actuator duty cycle—all while maintaining a state of minimum mechanical power consumption. In SEA architectures, we demonstrated how a range of additional power consumption metrics—including electrical resistive power losses—also remained invariant over a space of nonlinear elasticity. These principles open up a wide range of possibilities for biomimetic propulsion system design: we highlight, in particular, the possibility of designing an FW-MAV system using only a unidirectional linear actuator—e.g. a single solenoid, pneumatic cylinder, or micro-combustion cylinder [49]—to generate energetically optimal resonant oscillations. Unidirectional actuators of this form may show improved fuel-weight ratio relative to the current paradigm of battery-operated piezoelectric or DC motor actuation [45]. In this way, the one-way drive systems—and the elastic-bound principles more broadly—provide avenues for the design of novel biomimetic propulsion systems.

4.3 Implications for solving absolute-work minimisation problems

Optimisation problems, involving the minimisation of absolute work, or power, can sometimes be difficult to solve: the non-smoothness of the absolute-value function can impede numerical optimisation methods [40, 41, 63]. Our analysis approach directly tackles one class of these difficult problems, yielding solutions that are (**i**) accessible analytically, without calculus of optimisation, and (**ii**) simultaneously available for a range of different non-smooth mechanical power metrics (Sect. 2.1). Our analysis approach is able to bypass problems of smoothness via the principle that, if the system net power is invariant with respect to a given parameter (e.g. structural elasticity), then an energetically optimal state (e.g. in absolute power) is described by the condition that the system power requirement should contain no negative power (i.e. global resonance).

This principle is generalisable. For instance, consider some general 1DOF system with a prescribed kinematic output $x(t)$, power requirement $P(t)$, and two power metrics: net power, $\overline{\mathrm{P}}$, and absolute power, $\overline{\mathrm{P}}_{|\cdot|}$, both defined over some $t \in [0, T]$. Consider $\boldsymbol{\lambda} \in \mathbb{R}^N$ to be a vector of N time-invariant configuration parameters, influencing (in general) both the output $x(t)$ and the power requirement $P(t)$, via continuous real-valued functions $\tilde{x}(\cdot)$ and $\tilde{P}(\cdot)$:

$$\begin{aligned} &x(t) = \tilde{x}(\boldsymbol{\lambda}, t), \quad P(t) = \tilde{P}(\boldsymbol{\lambda}, x(t)), \\ &\overline{\mathrm{P}}(\boldsymbol{\lambda}) = \int_0^T P(t)dt, \quad \overline{\mathrm{P}}_{|\cdot|}(\boldsymbol{\lambda}) = \int_0^T |P(t)|dt. \end{aligned} \tag{32}$$

Note that $\overline{\mathrm{P}}_{|\cdot|} \geq \overline{\mathrm{P}}$ under any conditions. In the elastic-bound analysis of Sect. 2, $\boldsymbol{\lambda}$ represented the infinite-dimensional parameter space of all possible continuous elastic load functions, $F_s(x)$. And by the particular structure of $\tilde{P}(\cdot)$, we could determine that $\overline{\mathrm{P}}$ (equivalent to $P_{(a)}$ in Sect. 1) was independent of $F_s(x)$. Now, in this more general case, $\overline{\mathrm{P}}$ is not generally independent of $\boldsymbol{\lambda}$. But, assume we can identify a region, Ω, in the configuration space, $\Omega \subseteq \mathbb{R}^N$, such that over $\boldsymbol{\lambda} \in \Omega$, the net power $\overline{\mathrm{P}}$ is constant (i.e. Ω is a level set in $\overline{\mathrm{P}}$). Then, if there exist any $\boldsymbol{\lambda}^* \in \Omega$ satisfying $\overline{\mathrm{P}}_{|\cdot|}(\boldsymbol{\lambda}^*) = \overline{\mathrm{P}}(\boldsymbol{\lambda}^*)$, then, at these $\boldsymbol{\lambda}^*$, the absolute power $\overline{\mathrm{P}}_{|\cdot|}$ is minimised over Ω. In addition, $\overline{\mathrm{P}}_{|\cdot|} = \overline{\mathrm{P}}$ implies $P(t) \geq 0$, $\forall t \in [0, T]$ (i.e. no negative power): this latter condition also defines $\boldsymbol{\lambda}^*$.

This principle is an abstract statement of the logic used in Sects. 2.2–2.3. As a practical application: consider $\boldsymbol{\lambda}$ as the parameters describing the gait of a legged robot. If we can (**i**) construct a level set of gait parameters (Ω such that $\boldsymbol{\lambda} \in \Omega$ represents constant net power, $\overline{\mathrm{P}}$); and (**ii**) find the state of no negative work within the level set ($\boldsymbol{\lambda}^* \in \Omega$ such that $P(t) \geq 0$, $\forall t$); then this state, $\boldsymbol{\lambda}^*$, represents an energetically optimal gait over Ω. This provides an alternative, unstudied, approach to gait optimisation that does not rely on any calculus of optimisation. This approach may generalise to other absolute-work minimisation problems,

potentially including minimisation problems in non-mechanical work or power metrics.

4.4 Implications for the role of structural elasticity in biological propulsion systems

It is reasonably common, as a first-order approximation, to analyse the energetic behaviour of biological propulsion systems, such as insect flight motors, in terms of linear elasticity and linear resonance [17, 95–97]. However, more detailed structural analysis of insect flight motors reveals increasing evidence for the presence of nonlinear elasticities [14, 15]. The energetic effects of these nonlinearities are unclear—but our theoretical analysis sheds some light on the space of possibilities. We have demonstrated that such nonlinear elasticity can be consistent with energetic optimality, even in a system which is otherwise completely linear. In practical terms: the postulate that biological propulsion systems have evolved to be energetically optimal does not necessitate that they involve linear elasticity or linear resonance—*even if* the system is otherwise completely linear (linear inertia, dissipation, etc.). And further: in Sect. 3 we demonstrated that nonlinear elasticities can be used to control a wide range of system properties—e.g. actuator duty cycle, system equilibria—while maintaining energetic optimality. This form of control is available, at a state of energetic neutrality, even in dissipation-dominated systems (e.g. micro-swimmers), for which no resonant energy savings are possible. In biological propulsion systems, the role of structural elasticity in controlling these system properties (e.g. creating equilibria, synchronising load requirements with muscular capability) may be just as important as its role in saving energy via resonance. Our theoretical results provide a new avenue for characterising the role of elasticity in such systems.

4.5 Future directions

The analysis that we have presented in this paper shows several avenues for further theoretical and practical development. The limitations of the analysis indicate directions for theoretical development: extensions to more complex and more realistic SEA models [22–24]; extension to multi-degree-of-freedom models; extensions to non-invertible elasticities in SEA systems; and extensions to optimising viscoelastic elements. Also of significant relevance are approaches to considering actuator constraints, and/or additional optimisation objectives: whether via further work-loop analysis, or via the integration of convex-optimisation techniques, as discussed in Sect. 2.4. On a practical front: applying our technique to realistic systems requires a precise knowledge of the system dynamics, including the system dissipation—an aspect of the dynamics that may be particularly uncertain. Devising control architectures for locating and controlling these global-resonant states in uncertain systems is a topic of key practical relevance. Linear and nonlinear optimal control theory may be one direction towards constructing these control architectures. Another direction may be the study of insect flight motors control [98, 99]: elucidating the energetic role of known nonlinear elasticities in the insect flight motor might both inspire biomimetic forms of energetically optimal biomimetic propulsion system and shed light into the mechanical principles underlying insect flight.

5 Conclusions

In this work, we have presented a simple, general, and intuitive principle for constructing energetically optimal elasticities, in a range of general dynamical systems. This principle is based on elastic bounds within a system work loop and has diverse implications. It applies to a wide range of systems, linear and nonlinear, with parallel-elastic or series-elastic actuation, under conditions of imperfect actuator energy regeneration. It extends, in many ways, further into the energetic behaviour of the system and can be used to optimise more complex metrics of power consumption (e.g. metabolic, or electrical metrics). It provides a new method for designing energetically optimal nonlinear systems, allowing design control of a range of system properties—actuator duty cycle, system equilibrium location, quasistatic behaviour, and more; all while resonant energy savings are maintained. And, finally, it provides avenues for the design of radically novel biomimetic propulsion systems: energetically optimal systems actuated by unidirectional linear actuators, such as single solenoids or micro-combustion cylinders. Overall, this work-loop approach and associated principles are fundamental contributions to the study of energetic optimality in forced dynamical

systems. They offer several promising avenues for further development—including generalisation and extension of the fundamental principle, and practical application in a wide range of systems and contexts.

Acknowledgements This work was supported by the Azrieli Foundation Faculty Fellowship the Israel Ministry of Science and Technology, and the Israel Science Foundation (Grant No. 1851/17). AP was additionally supported by the Jerusalem Brain Community Post-Doctoral Fellowship.

Data availability No datasets were generated or utilised in this study.

Declarations

Conflict of interest The authors declare that they have no conflict of interest.

Appendix

A.1 Example constructions in PEA systems

For illustration, we derive specific forms of $G^{\pm}(x)$, and the elastic-bound condition, for two different PEA systems. First, consider a linear 1DOF PEA system, with time variable t, displacement x, inertia m, and dissipation coefficient c (Fig. 2, main text). The system is driven by an actuator, generating simple harmonic oscillation, amplitude $\hat{x}$:

$$\begin{aligned} &x(t) = \hat{x}\cos(\omega t), \dot{x}(t) = -\hat{x}\omega\sin(\omega t),\\ &\ddot{x}(t) = -\hat{x}\omega^2\cos(\omega t), \end{aligned} \tag{A.1.1}$$

The required actuator load for this oscillation, inelastic (G) and elastic (F), is given by:

$$\begin{aligned} &G(t) = m\ddot{x}(t) + c\dot{x}(t),\\ &F(t) = m\ddot{x}(t) + c\dot{x}(t) + F_s(x(t)), \end{aligned} \tag{A.1.2}$$

thus:

$$\begin{aligned} &G(t) = -m\hat{x}\omega^2\cos(\omega t) - c\hat{x}\omega\sin(\omega t),\\ &F(t) = -m\hat{x}\omega^2\cos(\omega t) - c\hat{x}\omega\sin(\omega t) + F_s(x(t)). \end{aligned} \tag{A.1.3}$$

Parameterising $G(t)$ and $F(t)$ in terms of $x(t) = \hat{x}\cos(\omega t)$, and splitting into two solutions (arcs) we have:

$$\begin{aligned} &G^{\pm}(x) = -m\omega^2 x \pm c\omega\sqrt{\hat{x}^2 - x^2}.\\ &F^{\pm}(x) = F_s(x) - m\omega^2 x \pm c\omega\sqrt{\hat{x}^2 - x^2}. \end{aligned} \tag{A.1.4}$$

The elastic-bound conditions then read: for $x \in [-\hat{x}, \hat{x}]$,

$$\begin{aligned} -m\omega^2 x - c\omega\sqrt{\hat{x}^2 - x^2} \leq\ &- F_s(x) \leq\ - m\omega^2 x\\ &+ c\omega\sqrt{\hat{x}^2 - x^2}. \end{aligned} \tag{A.1.5}$$

Optimal linear, cubic, and quintic elasticities—if they exist, which is dependent on the system parameters—are thus:

$$\begin{aligned} &F_{s,1}(x) = m\omega^2 x,\\ &F_{s,3}(x) = m\omega^2 x^3/\hat{x}^2,\\ &F_{s,5}(x) = m\omega^2 x^5/\hat{x}^4. \end{aligned} \tag{A.1.6}$$

Note that there is no more than one of each such optimal elasticity in this, or any other, system: one pure-linear, one cubic, etc. More broadly, we may define two families of optimal polynomial elasticities, interpolated linear-cubic and linear-quintic profiles, respectively:

$$\begin{aligned} &F_{s,1,3}(x,\alpha) = (1-\alpha)m\omega^2 x + \alpha m\omega^2 x^3/\hat{x}^2, \alpha \in [0,1],\\ &F_{s,1,5}(x,\beta) = (1-\beta)m\omega^2 x + \beta m\omega^2 x^5/\hat{x}^4, \beta \in [0,1]. \end{aligned} \tag{A.1.7}$$

The states $\alpha = 0$ and $\beta = 0$ represent linear profiles; and $\alpha = 1$ and $\beta = 1$, purely cubic and quintic profiles, respectively.

Second, consider a nonlinear 1DOF PEA system, undergoing the same simple-harmonic motion, but with quadratic damping—a simplified model of an insect flight motor:

$$\begin{aligned} &G(t) = m\ddot{x}(t) + \mathrm{sign}(\dot{x}(t))c\dot{x}(t)^2,\\ &F(t) = m\ddot{x}(t) + \mathrm{sign}(\dot{x}(t))c\dot{x}(t)^2 + F_s(x(t)), \end{aligned} \tag{A.1.8}$$

thus:

$$\begin{aligned} &G(t) = -m\hat{x}\omega^2\cos(\omega t) - \mathrm{sign}(\sin(\omega t))c\hat{x}^2\omega^2\sin^2(\omega t),\\ &F(t) = -m\hat{x}\omega^2\cos(\omega t) - \mathrm{sign}(\sin(\omega t))c\hat{x}^2\omega^2\sin^2(\omega t)\\ &\qquad + F_s(x(t)). \end{aligned} \tag{A.1.9}$$

Parameterising $G(t)$ and $F(t)$ in terms of $x(t) = \hat{x}\cos(\omega t)$ and splitting into two solutions (arcs), we have:

$$G^{\pm}(x) = -m\omega^2 x \pm c\omega^2\left(x^2 - \hat{x}^2\right),$$
$$F^{\pm}(x) = -m\omega^2 x \pm c\omega^2\left(x^2 - \hat{x}^2\right) + F_s(x(t)). \tag{A.1.10}$$

The elastic-bound conditions then read: for $x \in [-\hat{x}, \hat{x}]$,

$$-m\omega^2 x - c\omega^2\left(x^2 - \hat{x}^2\right) \leq -F_s(x) \leq -m\omega^2 x + c\omega^2\left(x^2 - \hat{x}^2\right). \tag{A.1.11}$$

Note that, because linear inertia and harmonic motion is common to both systems considered in this section, the optimal elastic profiles, if they exist, are the identical (identical optimal cubic elasticity, etc., as per Eqs. A.1.6, A.1.7).

A.2 Example constructions in SEA systems

For illustration, we derive specific forms of $X^{\pm}(x)$ and the associated elastic optimality condition, for an SEA system. Consider a linear, 1DOF, SEA, system, with time variable t, displacement x, inertia m, and dissipation coefficient c (per Fig. 4, main text). The system is driven by an actuator, generating simple harmonic oscillation, amplitude $\hat{x}$:

$$x(t) = \hat{x}\cos(\omega t), \dot{x}(t) = -\hat{x}\omega\sin(\omega t),$$
$$\ddot{x}(t) = -\hat{x}\omega^2\cos(\omega t), \tag{A.2.1}$$

The equation of motion for this system is:

$$m\ddot{x}(t) + c\dot{x}(t) = F_s(u(t) - x(t)), \tag{A.2.2}$$

and thus provided that $F_s(\cdot)$ is invertible, the required actuator displacement, $u(t)$, and actuator load, are given by apply $F_s^{-1}(\cdot)$ to Eq. A.2.2:

$$u(t) = x(t) + F_s^{-1}(m\ddot{x}(t) + c\dot{x}(t)),$$
$$F(t) = F_s(u(t) - x(t)) = m\ddot{x}(t) + c\dot{x}(t). \tag{A.2.3}$$

It follows that the actuator displacement requirement may be alternately cast as:

$$u(t) = x(t) + F_s^{-1}(F(t)), \tag{A.2.4}$$

To reformulate this requirement as $u(F)$, we must reformulate $x(t)$ in terms of F. From the definition of the actuator load, we have:

$$F(t) = -m\hat{x}\omega^2\cos(\omega t) - c\hat{x}\omega\sin(\omega t), \tag{A.2.5}$$

and thus, as with the PEA, a work loop representation, F-x:

$$F^{\pm}(x) = -m\omega^2 x \pm c\omega\sqrt{\hat{x}^2 - x^2}. \tag{A.2.6}$$

To invert this into a loop x-F, we go through the following process. Manipulating the root term in both $F^{+}(x)$ and $F^{-}(x)$ yields a single multivariable polynomial, describing the elliptical shape of the work loop, which can be solved for either F or x:

$$\left(m^2\omega^4 + c^2\omega^2\right)x^2 + 2Fm\omega^2 x + \left(F^2 - c^2\omega^2\hat{x}^2\right) = 0. \tag{A.2.7}$$

Note that F has replaced $F^{\pm}$ now that these branches are unified. The solution to this polynomial, in terms of x, are the functions we denote $X^{\pm}(F)$:

$$X^{\pm}(F) = \frac{-mF \pm \frac{c}{\omega}\sqrt{\hat{x}^2\omega^2(m^2\omega^2 + c^2) - F^2}}{m^2\omega^2 + c^2}. \tag{A.2.8}$$

The appropriate F-range for $X^{\pm}(F)$, $\left[-\hat{F}, \hat{F}\right]$, is given by the extrema of Eq. A.2.6:

$$\hat{F} = \omega\hat{x}\sqrt{m^2\omega^2 + c^2}. \tag{A.2.9}$$

The derivatives $X'^{\pm}(F)$ can be computed directly from Eq. A.2.8, as:

$$X'^{\pm}(F) = \frac{1}{m^2\omega^2 + c^2}\left(-m \mp \frac{cF}{\omega\sqrt{\hat{x}^2\omega^2(m^2\omega^2 + c^2) - F^2}}\right), \tag{A.2.10}$$

and the elastic bound-conditions read:

$$X'^{-}(F) \leq -\left(F_s^{-1}\right)'(F) \leq X'^{+}(F), \forall F \in [F_1, 0],$$
$$X'^{+}(F) \leq -\left(F_s^{-1}\right)'(F) \leq X'^{-}(F), \forall F \in [0, F_2]. \tag{A.2.11}$$

We note that this state condition can be fulfilled by some $F_s^{-1}(F)$: the optimal state is accessible (Sect. 2.3.4). More specifically:

$$X'^{-}(0) = X'^{+}(0) = \frac{-m}{m^2\omega^2 + c^2}$$
$$\therefore\left(F_{s,lin}^{-1}\right)'(0) = \frac{m}{m^2\omega^2 + c^2}, \tag{A.2.11}$$

where $F_{s,1}(\cdot)$ is the system optimal linear elasticity, alternately expressible as:

$$F_{s,lin}(u-x) = \frac{m^2\omega^2 + c^2}{m}(u-x). \tag{A.2.11}$$

A.3 Proof of mechanical power optimality in PEA systems

In this section, we prove the PEA elastic optimality results that we have utilised in the main text, prior to this point in the appendix. We begin at the formulation of the system as per the work loop of Eq. 7:

$$\begin{aligned} G^{\pm}(x) &= G_{\mathrm{mid}}(x) \pm G_{\mathrm{arc}}(x), \\ F^{\pm}(x) &= G_{\mathrm{mid}}(x) \pm G_{\mathrm{arc}}(x) + F_s(x), \end{aligned} \tag{A.3.1}$$

over $x \in [x_1, x_2]$, with $G_{\mathrm{arc}}(x) > 0$. If a system can be formulated as a work loop of this form, respecting the condition that the loop must be a simple closed curve, no more than bivalued at any x, and showing net power dissipation, then the system is admissible under this analysis.

First, consider evaluating the four integrals of mechanical power, Eq. 8, for $F^{\pm}(x)$. For the net power, $\overline{\mathrm{P}}_{(\mathrm{a})}$, we have the result:

$$\overline{\mathrm{P}}_{(\mathrm{a})} = \frac{1}{T}\int_{x_1}^{x_2} (F^+(x) - F^-(x))dx = \frac{2}{T}\int_{x_1}^{x_2} G_{\mathrm{arc}}(x)dx; \tag{A.3.2}$$

that is, the net power is unaffected by elasticity, $F_s(x)$, exactly as we would expect. For the other metrics, $\overline{\mathrm{P}}_{(\mathrm{b})}$, $\overline{\mathrm{P}}_{(\mathrm{c})}$, and $\overline{\mathrm{P}}_{(\mathrm{d})}$, however, no self-cancellation occurs, and a general dependency on elasticity, $F_s(x)$, remains. To gain further insight into the behaviour of these latter metrics, consider an alternative work loop parameterisation. Split $F^+(x)$ and $F^-(x)$ into four components, representing regions of positive (A) and negative (B) load:

$$\begin{aligned} &F^+(x) = A^+(x) - B^+(x), \quad F^-(x) = A^-(x) - B^-(x), \\ &A^+(x) = F^+(x)[F^+(x) \geq 0]_{\shortparallel}, \quad A^-(x) = F^-(x)[F^-(x) \geq 0]_{\shortparallel}, \\ &B^+(x) = -F^+(x)[F^+(x) \leq 0]_{\shortparallel}, \quad B^-(x) = -F^-(x)[F^-(x) \leq 0]_{\shortparallel}. \end{aligned} \tag{A.3.4}$$

Thus, $A^{\pm}(x), B^{\pm}(x) \geq 0, \forall x$, and individual power integrals for each component are necessarily positive:

$$\begin{aligned} W(I) &= \frac{1}{T}\int_{x_1}^{x_2} I(x)dx \geq 0, I(x) \\ &\in \{A^+(x), B^+(x), A^-(x), B^-(x)\}. \end{aligned} \tag{A.3.5}$$

This allows evaluation of the power metrics, Eq. 8, in terms of these $W(I)$. For the net power, $\overline{\mathrm{P}}_{(\mathrm{a})}$, we have the result:

$$\overline{\mathrm{P}}_{(\mathrm{a})} = W(A^+) + W(B^-) - W(A^-) - W(B^+), \tag{A.3.6}$$

where the terms $W(A^-)$ and $W(B^+)$ serve to reduce the actuator power consumption (via storage and release of negative power). We also have explicit results for $\overline{\mathrm{P}}_{(\mathrm{b})}$, $\overline{\mathrm{P}}_{(\mathrm{c})}$ and $\overline{\mathrm{P}}_{(\mathrm{d})}$:

$$\begin{aligned} \overline{\mathrm{P}}_{(\mathrm{b})} &= W(A^+) + W(B^-) + W(A^-) + W(B^+), \\ \overline{\mathrm{P}}_{(\mathrm{c})} &= W(A^+) + W(B^-), \\ \overline{\mathrm{P}}_{(\mathrm{d})} &= W(A^+) + W(B^-) - W(A^-) - W(B^+) + W_Q, \end{aligned} \tag{A.3.7}$$

with the special penalty integral for $\overline{\mathrm{P}}_{(\mathrm{d})}$:

$$\begin{aligned} W_Q = &\frac{1}{T}\int_{x_1}^{x_2} Q^+F^+[F^+ \leq 0]_{\shortparallel}dx \\ &+ \frac{1}{T}\int_{x_1}^{x_2} Q^-F^-[F^- \geq 0]_{\shortparallel}dx. \end{aligned} \tag{A.3.8}$$

These explicit forms have several implications, representable in the form of the following inequalities, valid $\forall F^{\pm}(x)$:

$$\begin{aligned} \overline{\mathrm{P}}_{(\mathrm{b})} &\geq \overline{\mathrm{P}}_{(\mathrm{a})}, \\ \overline{\mathrm{P}}_{(\mathrm{c})} &\geq \overline{\mathrm{P}}_{(\mathrm{a})}, \\ \overline{\mathrm{P}}_{(\mathrm{b})} &\geq \overline{\mathrm{P}}_{(\mathrm{c})}, \\ \overline{\mathrm{P}}_{(\mathrm{d})} &\geq \overline{\mathrm{P}}_{(\mathrm{a})}, \end{aligned} \tag{A.3.9}$$

these results can be seen from the fact that $W(I) \geq 0, \forall I(x)$. In the case of $\overline{\mathrm{P}}_{(\mathrm{d})} \geq \overline{\mathrm{P}}_{(\mathrm{a})}$, from the fact that $Q^{\pm}(x) > 0$ necessitates $W_Q \geq 0$.

Synthesising the information from Eqs. A.3.2 and A.3.9 yields the following conclusions. From Eq. A.3.2, $\overline{\mathrm{P}}_{(\mathrm{a})}$ is independent of $F_s(x)$, whereas $\overline{\mathrm{P}}_{(\mathrm{b})}$, $\overline{\mathrm{P}}_{(\mathrm{c})}$, and $\overline{\mathrm{P}}_{(\mathrm{d})}$ are (in general) dependent. From Eq. A.3.9, the minimum possible value that $\overline{\mathrm{P}}_{(\mathrm{b})}$, $\overline{\mathrm{P}}_{(\mathrm{c})}$ and $\overline{\mathrm{P}}_{(\mathrm{d})}$ can take, under any $F_s(x)$, is this independent

value of $\overline{\mathrm{P}}_{(\mathrm{a})}$. There is no immediate guarantee that this minimum is attainable, but we may explore the conditions for it to be attained. Given $W(I) \geq 0, \forall I(x)$:

$$\begin{aligned}
&\overline{\mathrm{P}}_{(\mathrm{b})} = \overline{\mathrm{P}}_{(\mathrm{a})} \Rightarrow W(A^-) + W(B^+) = 0 \Rightarrow W(A^-) = W(B^+) = 0,\\
&\overline{\mathrm{P}}_{(\mathrm{c})} = \overline{\mathrm{P}}_{(\mathrm{a})} \Rightarrow W(A^-) + W(B^+) = 0 \Rightarrow W(A^-) = W(B^+) = 0,\\
&\overline{\mathrm{P}}_{(\mathrm{d})} = \overline{\mathrm{P}}_{(\mathrm{a})} \Rightarrow W_Q = 0.
\end{aligned} \tag{A.3.10}$$

Consider these two sets of conditions separately. For $\overline{\mathrm{P}}_{(\mathrm{b})}$ and $\overline{\mathrm{P}}_{(\mathrm{c})}$, given that $A^-(x)$ and $B^+(x)$ cannot change sign (Eq. A.3.4), the integral condition $W(A^-) = W(B^+) = 0$ implies the functional condition $A^-(x) = B^+(x) = 0, \forall x$; that is, $\forall x$:

$$\begin{aligned}
&F^+(x)[F^+(x) \leq 0]_{\|} = 0,\\
&F^-(x)[F^-(x) \geq 0]_{\|} = 0.
\end{aligned} \tag{A.3.11}$$

For $\overline{\mathrm{P}}_{(\mathrm{d})}$, the condition $W_Q = 0$ implies directly the identical condition, that, $\forall x$:

$$\begin{aligned}
&F^+(x)[F^+(x) \leq 0]_{\|} = 0,\\
&F^-(x)[F^-(x) \geq 0]_{\|} = 0.
\end{aligned} \tag{A.3.12}$$

It follows that this single pair of conditions, Eqs. A.3.11 or A.3.12, ensure optimality in mechanical power both necessarily and sufficiently: they are the sole conditions to ensure that the inequalities of Eq. A.3.9 become equalities, and thus, the mechanical power metrics take their minimum possible values.

These conditions are interpretable in terms of $F_s(x)$, in the following way. To ensure that the expressions in Eqs. A.3.11 or A.3.12 are zero-valued $\forall x$, the following must be true:

$$\begin{aligned}
&\forall x \text{ either } F^+(x) = 0 \text{ or } [F^+(x) \leq 0]_{\|} = 0,\\
&\forall x \quad \text{either } F^-(x) = 0 \text{ or } [F^-(x) \geq 0]_{\|} = 0.
\end{aligned} \tag{A.3.13}$$

Computing the Iverson bracket, these conditions become:

$$\begin{aligned}
&\forall x \text{ either } F^+(x) = 0 \text{ or } F^+(x) > 0,\\
&\forall x \text{ either } F^-(x) = 0 \text{ or } F^-(x) < 0,
\end{aligned} \tag{A.3.14}$$

or, as two simple inequalities:

$$\begin{aligned}
&F^+(x) \geq 0,\\
&F^-(x) \leq 0.
\end{aligned} \tag{A.3.15}$$

This is the intuitive result of Sect. 2.2: the presence of negative power in the system, i.e. $F\dot{x} < 0$, necessarily implies that the system is suboptimal in terms of mechanical power.

What are the conditions on $F_s(x)$ to ensure Eq. A.3.15 is satisfied? This is simple to compute. As $F^{\pm}(x) = G^{\pm}(x) + F_s(x)$, by the system definition, Eq. A.3.1, it follows that:

$$\begin{aligned}
&G^+(x) + F_s(x) \geq 0,\\
&G^-(x) + F_s(x) \leq 0,
\end{aligned} \tag{A.3.16}$$

and thus:

$$G^-(x) \leq -F_s(x) \leq G^+(x), \tag{A.3.17}$$

which is the elastic-bound condition, Eq. 10 (Sect. 2.2). We have demonstrated that this condition is necessary and sufficient to ensure that any of the mechanical power metrics, $\overline{\mathrm{P}}_{(\mathrm{b})}$, $\overline{\mathrm{P}}_{(\mathrm{c})}$ and $\overline{\mathrm{P}}_{(\mathrm{d})}$, are minimised. Note that (**i**) we have computed this optimality condition analytically, not numerically, in contrast to most existing treatments of absolute-power minimisation [58, 59, 63]; (**ii**) we required no calculus of optimisation to do so: optimality can be deduced simply from the form of the power integrals in the F-x domain; and (**iii**) no differentiability requirements have been imposed on any system parameters. Work-loop analysis is a powerful tool for analysing the optimality of system parameters with respect to mechanical power consumption.

A.4 Proof of mechanical power optimality in SEA systems

We begin with a general SEA system defined as per Eq. 11. We then place the following restrictions, defining the admissibility of the system for our analysis. We require that there exist time-domain functions $x(t)$, $\dot{x}(t)$, $F(t)$, and $\dot{F}(t)$, all continuous and real-valued over all real-valued t, and periodic with period T. Consider the function $\dot{F}(t)$ in more detail. We define two sets of times, T^+ and T^-, in relation to this function: $T^+ = \{t : \dot{F}(t) < 0\}$, and $T^- = \{t : \dot{F}(t) \geq 0\}$. Note the association of "+" with "< 0" and "−" with "≥ 0" is intentional. We require that these sets of times exist. If they do, they are necessarily unique, and together span all t, i.e. $T^+ \cup T^- = \mathbb{R}$. We can then use these time windows to segment $\dot{F}(t)$ into two functions: $\dot{f}^+(t) = \dot{F}(t)$, defined for $t \in T^+$, and $\dot{f}^-(t) = \dot{F}(t)$, defined for $t \in T^-$. It

follows that $\dot{f}^+(t)<0$, $\forall t \in T^+$, and $\dot{f}^+(t)\geq 0$, $\forall t \in T^+$, and we may reconstruct $\dot{F}(t)$ as:

$$\dot{F}(t) = \begin{cases} \dot{f}^+(t) & t \in T^+, \\ \dot{f}^-(t) & t \in T^-. \end{cases} \tag{A.4.1}$$

We now apply the same process to $x(t)$, $\dot{x}(t)$ and $F(t)$:

$$x(t) = \begin{cases} x^+(t) & t \in T^+, \\ x^-(t) & t \in T^-, \end{cases} \dot{x}(t) = \begin{cases} \dot{x}^+(t) & t \in T^+, \\ \dot{x}^-(t) & t \in T^-, \end{cases}$$

$$F(t) = \begin{cases} f^+(t) & t \in T^+, \\ f^-(t) & t \in T^-, \end{cases} \tag{A.4.2}$$

defining $x^\pm(t)$, $\dot{x}^\pm(t)$ and $F^\pm(t)$. We require the following condition be satisfied by these functions: that the value of $x^+(t)$, $x^-(t)$, $\dot{x}^+(t)$ and $\dot{x}^-(t)$, at all t, must be uniquely defined by the value $F(t)$. In equivalent terms: $f^+(t)$ and $f^-(t)$ must be invertible: the periodic waveform $F(t)$ must be composed to two monotonic half cycles.

If this condition is satisfied, we may parameterise $x^\pm(t)$ and $\dot{x}^\pm(t)$ in terms of F:

$$x(t) = \begin{cases} X^+(F(t)) & t \in T^+, \\ X^-(F(t)) & t \in T^-, \end{cases} \dot{x}(t) = \begin{cases} \dot{X}^+(F(t)) & t \in T^+, \\ \dot{X}^-(F(t)) & t \in T^-, \end{cases}$$
$$\dot{F}(t) = \begin{cases} \dot{F}^+(F(t)) & t \in T^+, \\ \dot{F}^-(F(t)) & t \in T^-, \end{cases} \tag{A.4.3}$$

where $x^\pm(t)$ and $\dot{x}^\pm(t)$ have now been reformulated into the functions $X^\pm(F)$, $\dot{X}^\pm(F)$ and $F^\pm(F)$, defined over an interval in force, $F \in [F_1, F_2]$, where $F_1 = \min F(t)$ and $F_2 = \max F(t)$. The function $X^\pm(F)$ we will recognise as a work loop: $dx \cdot dF$ is the differential of work. The final condition which we require to be satisfied is: $X^+(F) \geq X^-(F), \forall F \in [F_1, F_2]$ (*NB*: the motivation behind the allocation of the superscript symbols, $\pm$). We note that the conditions $X^+(F_1) = X^-(F_1)$ and $X^+(F_2) = X^-(F_2)$ are already necessarily satisfied by nature of the continuity of $x(t)$.

If these conditions are satisfied, then we consider the system admissible for our analysis, and we may proceed. Consider an elastic element in the system, with elastic load profile $F_s(\delta)$, continuous, differentiable, and real-valued over all real-valued δ. We require that $F_s(\delta)$ be invertible. We may then express the SEA dynamics and power requirements (cf. Equation 12) as:

$$\begin{aligned} u(t) &= x(t) + F_s^{-1}(F(t)), \\ \dot{u}(t) &= \dot{x}(t) + \dot{F}(t)\left(F_s^{-1}\right)'(F(t)), \\ P(t) &= F(t)\dot{u}(t), \end{aligned} \tag{A.4.4}$$

where $\left(F_s^{-1}\right)'(F)$ denotes $\frac{d}{dF}F_s^{-1}(F)$. Note that we have used the differential relation.

$dF = \dot{F}dt$ to reformulate $\frac{d}{dt}F_s^{-1}(F)$ and $\dot{F}(t)\frac{d}{dF}F_s^{-1}(F)$. Using the sets of times, T^+ and T^-, we may segment these additional functions in the manner of Eq. A.4.2:

$$u(t) = \begin{cases} u^+(t) & t \in T^+, \\ u^-(t) & t \in T^-, \end{cases} \dot{u}(t) = \begin{cases} \dot{u}^+(t) & t \in T^+, \\ \dot{u}^-(t) & t \in T^-, \end{cases}$$
$$P(t) = F(t)\dot{u}(t), \tag{A.4.5}$$

and parameterise them in terms of F, in the manner of Eq. A.4.3:

$$u(t) = \begin{cases} U^+(F(t)) & t \in T^+, \\ U^-(F(t)) & t \in T^-, \end{cases} \dot{u}(t) = \begin{cases} \dot{U}^+(F(t)) & t \in T^+, \\ \dot{U}^-(F(t)) & t \in T^-, \end{cases}$$
$$P(t) = \begin{cases} P^+(F(t)) & t \in T^+, \\ P^-(F(t)) & t \in T^-, \end{cases} \tag{A.4.6}$$

Now, we can relate these segmented and parameterised functions to known system functions (Eqs. A.4.2 and A.4.3). Then, over $F \in [F_1, F_2]$:

$$\begin{aligned} u^\pm(t) &= x^\pm(t) + F_s^{-1}\left(f^\pm(t)\right), \\ \dot{u}^\pm(t) &= \dot{x}^\pm(t) + \dot{f}^\pm(t) \cdot \left(F_s^{-1}\right)'\left(f^\pm(t)\right), \\ p^\pm(t) &= f^\pm(t) \cdot \left(\dot{x}^\pm(t) + \dot{f}^\pm(t)\left(F_s^{-1}\right)'\left(f^\pm(t)\right)\right), \\ U^\pm(F) &= X^\pm(F) + F_s^{-1}(F), \\ \dot{U}^\pm(F) &= \dot{X}^\pm(F) + \dot{F}^\pm(F) \cdot \left(F_s^{-1}\right)'(F), \\ P^\pm(F) &= F \cdot \left(\dot{X}^\pm(F) + \dot{F}^\pm(F) \cdot \left(F_s^{-1}\right)'(F)\right). \end{aligned} \tag{A.4.7}$$

In addition, we can define the work-loop tangent functions, $X'^\pm(F) = \frac{d}{dF}X^\pm(F)$ and $U'^\pm(F) = \frac{d}{dF}U^\pm(F)$, where:

$$X'^\pm(F) = \frac{\dot{X}^+(F)}{\dot{F}^+(F)}, U'^\pm(F) = X'^\pm(F) + \left(F_s^{-1}\right)'(F), \tag{A.4.8}$$

and thus:

$$P^{\pm}(F) = F \cdot \dot{F}^{\pm}(F) \cdot \left(X'^{\pm}(F) + \left(F_s^{-1}\right)'(F) \right). \tag{A.4.9}$$

We are now able to evaluate the actuator power consumption metrics (**a**)–(**d**) (Sect. 2.1) in terms of $P^{\pm}(F)$. For the net power, metric (**a**):

$$\begin{aligned} \overline{\mathrm{P}}_{(\mathrm{a})} &= \frac{1}{T}\int_0^T P(t)dt \\ &= \frac{1}{T}\left(\int_{t\in T^+} p^+(t)dt + \int_{t\in T^-} p^-(t)dt \right) \\ &= \frac{1}{T}\left(\int_{F_2}^{F_1} \frac{P^+(F)}{\dot{F}^+(F)}dF + \int_{F_1}^{F_2} \frac{P^-(F)}{\dot{F}^-(F)}dF \right), \end{aligned} \tag{A.4.10}$$

where, flipping limits; $[F_2, F_1]$ to $[F_1, F_2]$, we obtain:

$$\overline{\mathrm{P}}_{(\mathrm{a})} = \frac{1}{T}\left(\int_{F_1}^{F_2} F \cdot (X'^{-}(F) - X'^{+}(F))dF \right). \tag{A.4.11}$$

We require that the sets of time $T^{\pm}$ permit an adequate definition of integration (i.e. they are composed of continuous intervals). We observe that $\overline{\mathrm{P}}_{(\mathrm{a})}$ is independent of $F_s(\delta)$: the net power is unaltered by elasticity. We can perform the same process for $\overline{\mathrm{P}}_{(\mathrm{d})}$ and thereby recover both $\overline{\mathrm{P}}_{(\mathrm{b})}$ and $\overline{\mathrm{P}}_{(\mathrm{c})}$, as we already know that they are special cases of $\overline{\mathrm{P}}_{(\mathrm{d})}$. Evaluating $\overline{\mathrm{P}}_{(\mathrm{d})}$, we obtain:

$$\begin{aligned} \overline{\mathrm{P}}_{(\mathrm{d})} &= \frac{1}{T}\int_0^T \left(P(t) + Q(t)|P(t)|[P(t)\le 0]_{\mathbb{I}}\right)dt \\ &== \frac{1}{T}\int_{t\in T^+} \left(p^+(t) + q^+(t)|p^+(t)|[p^+(t)\le 0]_{\mathbb{I}}\right)dt \\ &\quad + \frac{1}{T}\int_{t\in T^-} \left(p^-(t) + q^-(t)|p^-(t)|[p^-(t)\le 0]_{\mathbb{I}}\right)dt, \end{aligned} \tag{A.4.12}$$

and thus $\overline{\mathrm{P}}_{(\mathrm{d})} = \overline{\mathrm{P}}_{(\mathrm{a})} + \Delta\overline{P}$, where:

$$\Delta\overline{P} = \frac{1}{T}\int_{F_1}^{F_2} \left(\frac{Q^-(F)|P^-(F)|[P^-(F)\le 0]_{\mathbb{I}}}{\dot{F}^-(F)} - \frac{Q^+(F)|P^+(F)|[P^+(F)\le 0]_{\mathbb{I}}}{\dot{F}^+(F)} \right)dF. \tag{A.4.13}$$

We can see that $\Delta\overline{P} \ge 0$ in any system that we have defined:

(**i**) For power metric (**d**), $Q(t) > 0$, $\forall t$, and so $Q^{\pm}(F) > 0$, $\forall F$.

(**ii**) $\left|P^{\pm}(F)\right| \ge 0$, $\forall F$, and $[P^-(F)\le 0]_{\mathbb{I}} \ge 0$, $\forall F$, necessarily.

(**iii**) $\dot{F}^-(F) \ge 0$ and $\dot{F}^+(F) < 0$, by our construction.

Thus $\Delta\overline{P} \ge 0$. Physically, this is a simple restatement of the principle that the actuator power consumption is always greater than or equal to the net work—as studied also in "Appendix A.3". It follows that if we can use elasticity, $F_s(\delta)$, to ensure that $\Delta\overline{P} = 0$ (i.e. $\overline{\mathrm{P}}_{(\mathrm{a})} = \overline{\mathrm{P}}_{(\mathrm{d})}$) then we will have reached a state of minimum $\overline{\mathrm{P}}_{(\mathrm{d})}$ w.r.t. elasticity. Based on the time-domain formulation of $\overline{\mathrm{P}}_{(\mathrm{a})}$ and $\overline{\mathrm{P}}_{(\mathrm{d})}$, we can see that $\overline{\mathrm{P}}_{(\mathrm{a})} = \overline{\mathrm{P}}_{(\mathrm{d})}$ when $P(t) \ge 0$, $\forall t$—i.e. the absence of negative work; and the global resonance condition of Ma and Zhang [50–53]. What elasticity, $F_s(\delta)$, will ensure that this condition is satisfied? If $P(t) \ge 0$, $\forall t$, then $p^+(t) \ge 0, \forall t \in T^+$ and $p^-(t) \ge 0, \forall t \in T^-$; and thus, $P^{\pm}(F) \ge 0$, $\forall F \in [F_1, F_2]$. Hence:

$$F \cdot \dot{F}^{\pm}(F) \cdot \left(X'^{\pm}(F) + \left(F_s^{-1}\right)'(F) \right) \ge 0, \forall F \in [F_1, F_2]. \tag{A.4.12}$$

We may disassemble this condition according to the signs of F and $\dot{F}^{\pm}(F)$:

(**A**) Consider $F > 0$, i.e. $F \in (0, F_2]$. Then:

$$\dot{F}^{\pm}(F) \cdot \left(X'^{\pm}(F) + \left(F_s^{-1}\right)'(F) \right) \ge 0, \forall F \in (0, F_2], \tag{A.4.13}$$

(**A.i**) Take $\dot{F}^+(F) < 0$, over $X'^+(F)$. Then:

$$-\left(F_s^{-1}\right)'(F) \ge X'^+(F), \forall F \in (0, F_2], \tag{A.4.14}$$

(**A.ii**) Or, take instead $\dot{F}^-(F) > 0, \dot{F}^-(F) \ne 0$, over $X'^-(F)$. Then:

$$-\left(F_s^{-1}\right)'(F) \le X'^-(F), \forall F \in (0, F_2], \dot{F}^-(F) \ne 0. \tag{A.4.15}$$

(**B**) Consider the case $F < 0$, i.e. $F \in [F_1, 0)$. Then:

$$\dot{F}^{\pm}(F)\cdot\left(X'^{\pm}(F)+\left(F_s^{-1}\right)'(F)\right)\leq 0,\forall F\in[F_1,0), \tag{A.4.16}$$

(**B.i**) Take $\dot{F}^{+}(F)<0$, over $X'^{+}(F)$. Then:

$$-\left(F_s^{-1}\right)'(F)\leq X'^{+}(F),\forall F\in(0,F_2], \tag{A.4.17}$$

(**B.ii**) Or, take instead $\dot{F}^{-}(F)>0,\dot{F}^{-}(F)\neq 0$, over $X'^{-}(F)$. Then:

$$-\left(F_s^{-1}\right)'(F)\geq X'^{-}(F),\forall F\in(0,F_2],\dot{F}^{-}(F)\neq 0. \tag{A.4.18}$$

(**C**) Consider $F=0$ and/or $\dot{F}^{-}(F)=0$.

Then the elasticity is unbounded. However, note that as $F=\delta F\to 0$, from both below and above zero, then we have the four limits:

$$\begin{aligned}X'^{-}(\delta F)\leq&-\left(F_s^{-1}\right)'(\delta F)\leq X'^{+}(\delta F),\delta F\to 0,\delta F<0,\\ X'^{+}(\delta F)\leq&-\left(F_s^{-1}\right)'(\delta F)\leq X'^{-}(\delta F),\delta F\to 0,\delta F>0,\end{aligned} \tag{A.4.19}$$

and thus, if the values $X'^{\pm}(0)$ exist, then we require that $-\left(F_s^{-1}\right)'(0)=X'^{\pm}(0)$. This contrasts to the behaviour of these conditions as $\dot{F}=\delta\dot{F}\to 0$: there, $X'\to\infty$ (unless, $\dot{x}\to 0$ more rapidly), and so, in general, the optimal compliance will be unbounded in this limit.

Concatenating all these conditions, we obtain the elastic-bound conditions, Eq. 20:

$$\begin{aligned}X'^{-}(F)\leq&-\left(F_s^{-1}\right)'(F)\leq X'^{+}(F),\forall F\in[F_1,0];\\ X'^{+}(F)\leq&-\left(F_s^{-1}\right)'(F)\leq X'^{-}(F),\forall F\in[0,F_2].\end{aligned} \tag{A.4.20}$$

In this proof, we have demonstrated that these conditions are sufficient and necessary to ensure that any of the mechanical power metrics, $\overline{\mathrm{P}}_{(\mathrm{b})}$, $\overline{\mathrm{P}}_{(\mathrm{c})}$, and $\overline{\mathrm{P}}_{(\mathrm{d})}$, take the value of the net power, $\overline{\mathrm{P}}_{(\mathrm{a})}$—a value less than or equal to their minimum possible value over the space of $F_s(\cdot)$. However, as discussed in Sect. 2.3, it is possible that Eq. 20 cannot be satisfied by any linear or nonlinear elasticity, in which case the value of the net power, $\overline{\mathrm{P}}_{(\mathrm{a})}$, is always *less than* the minimum value(s) of $\overline{\mathrm{P}}_{(\mathrm{b})}$, $\overline{\mathrm{P}}_{(\mathrm{c})}$, and $\overline{\mathrm{P}}_{(\mathrm{d})}$ over the space of $F_s(\cdot)$. In this scenario, these minimum value(s) must be computed via some other method. The condition on $X'^{\pm}(F)$ that ensures that Eq. A.4.20 admits some solution for $\left(F_s^{-1}\right)'(F)$ is simply that:

$$\begin{aligned}X'^{+}(F)\geq X'^{-}(F),\forall F\in[F_1,0],\\ X'^{-}(F)\geq X'^{+}(F),\forall F\in[0,F_2],\end{aligned} \tag{A.4.21}$$

implying, at $F=0$, that $X'^{+}(0)=X'^{-}(0)$.

A.5 Proof of conditional absolute-load invariance in PEA systems.

The PEA elastic-bound conditions (Eq. 10) also define a region of invariance in the absolute load integral, $\overline{P}_{|F|}$, as per Sect. 2.4. Here we provide proof. Consider a general PEA system, as per Eq. 7, with its attendant conditions for admissibility. We may evaluate $\overline{\mathrm{P}}_{|F|}$ by segmenting $F(t)$ into two time-domain profiles, $F^{+}(t)$ following $F^{-}(t)$, without loss of generality, representing $F^{\pm}(x)$ in the time domain. The time T^{*} represents the transition between $F^{\pm}(t)$. Under an elasticity that is optimal in terms of mechanical power consumption, $F^{+}(t)\geq 0$ and $F^{-}(t)\leq 0$, and thus we have:

$$\overline{\mathrm{P}}_{|F|}\propto\frac{1}{T}\int_0^T|F(t)|dt=\frac{1}{T}\int_{T^*}^{T}F^{+}(t)dt-\frac{1}{T}\int_0^{T^*}F^{-}(t)dt. \tag{A.5.1}$$

Via the differential relation, $dt=1/\dot{x}dx$, we may recast this integral into an integral over x, with the velocity functions $\dot{x}^{+}(x)$ and $\dot{x}^{-}(x)$ representing the velocities associated with time windows $[T^{*},T]$ and $[0,T^{*}]$, respectively, matching $F^{\pm}(x)$. This yields:

$$\overline{\mathrm{P}}_{|F|}\propto\int_{x_1}^{x_2}\frac{F^{+}(x)}{\dot{x}^{+}(x)}dx+\int_{x_1}^{x_2}\frac{F^{-}(x)}{\dot{x}^{-}(x)}dx, \tag{A.5.2}$$

where, note, the negative sign arises because of the need to switch integration over the window $[x_2,x_1]$ to $[x_1,x_2]$. If, then, we have a symmetric waveform, $x(t)=x(T-t)$, $\forall t$, in the time-domain, or $\dot{x}^{+}(x)=-\dot{x}^{-}(x)=\dot{x}_{\mathrm{ref}}(x)>0$, $x\in[x_1,x_2]$ in the displacement domain, then we have:

$$\overline{\mathrm{P}}_{|F|}\propto\int_{x_1}^{x_2}\frac{F^{+}(x)-F^{-}(x)}{\dot{x}_{\mathrm{ref}}(x)}dx. \tag{A.5.3}$$

Under the definition of $F^{\pm}(x)$, this reduces to:

$$\overline{\mathrm{P}}_{|F|} \propto \int_{x_1}^{x_2} \frac{G_{\mathrm{arc}}(x)}{\dot{x}_{\mathrm{ref}}(x)}\, dx, \tag{A.5.4}$$

which is independent of $F_s(x)$. That is, under the waveform symmetry condition, $x(t) = x(T - t)$, $\forall t$, the metric $\overline{\mathrm{P}}_{|F|}$ is invariant under any elasticity satisfying Eq. 10.

References

1. Bujard, T., Giorgio-Serchi, F., Weymouth, G.D.: A resonant squid-inspired robot unlocks biological propulsive efficiency. Sci. Robot. 6, eabd2971 (2021). https://doi.org/10.1126/scirobotics.abd2971
2. Hoover, A., Miller, L.: A numerical study of the benefits of driving jellyfish bells at their natural frequency. J. Theor. Biol. **374**, 13–25 (2015). https://doi.org/10.1016/j.jtbi.2015.03.016
3. Hoover, A.P., Porras, A.J., Miller, L.A.: Pump or coast: the role of resonance and passive energy recapture in medusan swimming performance. J. Fluid Mech. **863**, 1031–1061 (2019). https://doi.org/10.1017/jfm.2018.1007
4. Hoover, A.P., Xu, N.W., Gemmell, B.J., Colin, S.P., Costello, J.H., Dabiri, J.O., Miller, L.A.: Neuromechanical wave resonance in jellyfish swimming. Proc. Natl. Acad. Sci. **118**, e2020025118 (2021). https://doi.org/10.1073/pnas.2020025118
5. Bhalla, A.P.S., Griffith, B.E., Patankar, N.A.: A Forced Damped Oscillation Framework for Undulatory Swimming Provides New Insights into How Propulsion Arises in Active and Passive Swimming. PLOS Comput. Biol. **9**, e1003097 (2013). https://doi.org/10.1371/journal.pcbi.1003097
6. Kohannim, S., Iwasaki, T.: Analytical insights into optimality and resonance in fish swimming. J. R. Soc. Interface. **11**, 20131073 (2014). https://doi.org/10.1098/rsif.2013.1073
7. Tytell, E.D., Hsu, C.-Y., Fauci, L.J.: The role of mechanical resonance in the neural control of swimming in fishes. Zoology **117**, 48–56 (2014). https://doi.org/10.1016/j.zool.2013.10.011
8. Demir, M., Salman, H.: Resonance in the response of the bacterial flagellar motor to thermal oscillations. Phys. Rev. E. **95**, 022419 (2017). https://doi.org/10.1103/PhysRevE.95.022419
9. Ling, F., Guo, H., Kanso, E.: Instability-driven oscillations of elastic microfilaments. J. R. Soc. Interface. **15**, 20180594 (2018). https://doi.org/10.1098/rsif.2018.0594
10. Ma, K.Y., Chirarattananon, P., Fuller, S.B., Wood, R.J.: Controlled Flight of a Biologically Inspired. Insect-Scale Robot. Science. **340**, 603–607 (2013)
11. Tu, Z., Fei, F., Deng, X.: Untethered Flight of an At-Scale Dual-motor Hummingbird Robot with Bio-inspired Decoupled Wings. IEEE Robot. Autom. Lett. 1–1 (2020). https://doi.org/10.1109/LRA.2020.2974717
12. Zhang, C., Rossi, C.: A review of compliant transmission mechanisms for bio-inspired flapping-wing micro air vehicles. Bioinspir. Biomim. **12**, 025005 (2017). https://doi.org/10.1088/1748-3190/aa58d3
13. Hrncir, M., Gravel, A.-I., Schorkopf, D.L.P., Schmidt, V.M., Zucchi, R., Barth, F.G.: Thoracic vibrations in stingless bees (Melipona seminigra): resonances of the thorax influence vibrations associated with flight but not those associated with sound production. J. Exp. Biol. **211**, 678–685 (2008). https://doi.org/10.1242/jeb.013920
14. Jankauski, M.A.: Measuring the frequency response of the honeybee thorax. Bioinspir. Biomim. **15**, 046002 (2020). https://doi.org/10.1088/1748-3190/ab835b
15. Gau, J., Gravish, N., Sponberg, S.: Indirect actuation reduces flight power requirements in *Manduca sexta* via elastic energy exchange. J. R. Soc. Interface. **16**, 20190543 (2019). https://doi.org/10.1098/rsif.2019.0543
16. Gau, J., Gemilere, R., (FM subteam), L.-V., Lynch, J., Gravish, N., Sponberg, S.: Rapid frequency modulation in a resonant system: aerial perturbation recovery in hawkmoths. Proc. R. Soc. B Biol. Sci. 288, 20210352 (2021). https://doi.org/10.1098/rspb.2021.0352
17. Lynch, J., Gau, J., Sponberg, S., Gravish, N.: Dimensional analysis of spring-wing systems reveals performance metrics for resonant flapping-wing flight. J. R. Soc. Interface. **18**, 20200888 (2021). https://doi.org/10.1098/rsif.2020.0888
18. Lehmann, F.O., Dickinson, M.H.: The control of wing kinematics and flight forces in fruit flies (Drosophila spp.). J. Exp. Biol. 201, 385 (1998). https://doi.org/10.1242/jeb.201.3.385
19. Deora, T., Singh, A.K., Sane, S.P.: Biomechanical basis of wing and haltere coordination in flies. Proc. Natl. Acad. Sci. **112**, 1481–1486 (2015). https://doi.org/10.1073/pnas.1412279112
20. Robertson, B.D., Sawicki, G.S.: Unconstrained muscle-tendon workloops indicate resonance tuning as a mechanism for elastic limb behavior during terrestrial locomotion. Proc. Natl. Acad. Sci. **112**, E5891–E5898 (2015). https://doi.org/10.1073/pnas.1500702112
21. Bauer, F., Römer, U., Fidlin, A., Seemann, W.: Optimization of energy efficiency of walking bipedal robots by use of elastic couplings in the form of mechanical springs. Nonlinear Dyn. **83**, 1275–1301 (2016). https://doi.org/10.1007/s11071-015-2402-9
22. Bolívar-Nieto, E.A., Summers, T., Gregg, R.D., Rezazadeh, S.: A convex optimization framework for robust-feasible series elastic actuators. Mechatronics **79**, 102635 (2021). https://doi.org/10.1016/j.mechatronics.2021.102635
23. Bolivar Nieto, E.A., Rezazadeh, S., Gregg, R.D.: Minimizing Energy Consumption and Peak Power of Series Elastic Actuators: A Convex Optimization Framework for Elastic Element Design. IEEEASME Trans. Mechatron. **24**, 1334–1345 (2019). https://doi.org/10.1109/TMECH.2019.2906887
24. Bolívar, E., Rezazadeh, S., Summers, T., Gregg, R.D.: Robust Optimal Design of Energy Efficient Series Elastic Actuators: Application to a Powered Prosthetic Ankle. In: 2019 IEEE 16th International Conference on Rehabilitation Robotics (ICORR). pp. 740–747. IEEE, Toronto, ON, Canada (2019)

25. Verstraten, T., Beckerle, P., Furnémont, R., Mathijssen, G., Vanderborght, B., Lefeber, D.: Series and Parallel Elastic Actuation: Impact of natural dynamics on power and energy consumption. Mech. Mach. Theory. **102**, 232–246 (2016). https://doi.org/10.1016/j.mechmachtheory.2016.04.004
26. Beckerle, P., Verstraten, T., Mathijssen, G., Furnemont, R., Vanderborght, B., Lefeber, D.: Series and Parallel Elastic Actuation: Influence of Operating Positions on Design and Control. IEEEASME Trans. Mechatron. **22**, 521–529 (2017). https://doi.org/10.1109/TMECH.2016.2621062
27. Verstraten, T., Geeroms, J., Mathijssen, G., Convens, B., Vanderborght, B., Lefeber, D.: Optimizing the power and energy consumption of powered prosthetic ankles with series and parallel elasticity. Mech. Mach. Theory. **116**, 419–432 (2017). https://doi.org/10.1016/j.mechmachtheory.2017.06.004
28. Beckerle, P., Stuhlenmiller, F., Rinderknecht, S.: Stiffness Control of Variable Serial Elastic Actuators: Energy Efficiency through Exploitation of Natural Dynamics. Actuators. **6**, 28 (2017). https://doi.org/10.3390/act6040028
29. Amara, V.D., Malzahn, J., Roozing, W., Tsagarakis, N.: Blending of Series-Parallel Compliant Actuation With Field Weakening Control for Explosive Motion Generation. IEEE Robot. Autom. Lett. **6**, 2076–2083 (2021). https://doi.org/10.1109/LRA.2021.3061066
30. Jordan, H.E.: Energy-Efficient Electric Motors and their Applications. Springer, Dordrecht, The Netherlands (1994)
31. Okyay, A., Khamesee, M.B., Erkorkmaz, K.: Design and Optimization of a Voice Coil Actuator for Precision Motion Applications. IEEE Trans. Magn. **51**, 1–10 (2015). https://doi.org/10.1109/TMAG.2014.2381160
32. Franco, E., Ayatullah, T., Sugiharto, A., Garriga-Casanovas, A., Virdyawan, V.: Nonlinear energy-based control of soft continuum pneumatic manipulators. Nonlinear Dyn. **106**, 229–253 (2021). https://doi.org/10.1007/s11071-021-06817-1
33. Kalita, B., Dwivedy, S.K.: Dynamic analysis of pneumatic artificial muscle (PAM) actuator for rehabilitation with principal parametric resonance condition. Nonlinear Dyn. **97**, 2271–2289 (2019). https://doi.org/10.1007/s11071-019-05122-2
34. Scheidl, R., Manhartsgruber, B.: On the Dynamic Behavior of Servo-Hydraulic Drives. Nonlinear Dyn. **17**, 247–268 (1998). https://doi.org/10.1023/A:1008348714791
35. Hattori, S., Hara, M., Nabae, H., Hwang, D., Higuchi, T.: Design of an impact drive actuator using a shape memory alloy wire. Sens. Actuators Phys. **219**, 47–57 (2014). https://doi.org/10.1016/j.sna.2014.08.013
36. van den Broek, D.M., Elwenspoek, M.: Explosive Micro-Bubble Actuator. In: TRANSDUCERS 2007 - 2007 International Solid-State Sensors, Actuators and Microsystems Conference. pp. 2441–2444. IEEE, Lyon (2007)
37. Dudley, R.: The Biomechanics of Insect Flight. Princeton University Press, Princeton, NJ (2002)
38. Maddock, L., Bone, Q., Rayner, J.M.V., Marine Biological Association of the United Kingdom, Society for Experimental Biology (Great Britain) eds: Mechanics and physiology of animal swimming. Cambridge University Press, Cambridge, UK (1994)
39. Berret, B., Chiovetto, E., Nori, F., Pozzo, T.: Evidence for Composite Cost Functions in Arm Movement Planning: An Inverse Optimal Control Approach. PLOS Comput. Biol. **7**, e1002183 (2011). https://doi.org/10.1371/journal.pcbi.1002183
40. Berret, B., Darlot, C., Jean, F., Pozzo, T., Papaxanthis, C., Gauthier, J.P.: The Inactivation Principle: Mathematical Solutions Minimizing the Absolute Work and Biological Implications for the Planning of Arm Movements. PLOS Comput. Biol. **4**, e1000194 (2008). https://doi.org/10.1371/journal.pcbi.1000194
41. Kelly, M.: An Introduction to Trajectory Optimization: How to Do Your Own Direct Collocation. SIAM Rev. **59**, 849–904 (2017). https://doi.org/10.1137/16M1062569
42. Verstraten, T., Mathijssen, G., Furnémont, R., Vanderborght, B., Lefeber, D.: Modeling and design of geared DC motors for energy efficiency: Comparison between theory and experiments. Mechatronics **30**, 198–213 (2015). https://doi.org/10.1016/j.mechatronics.2015.07.004
43. Gregg, R.D., Spong, M.W.: Reduction-based Control of Three-dimensional Bipedal Walking Robots. Int. J. Robot. Res. **29**, 680–702 (2010). https://doi.org/10.1177/0278364909104296
44. Verhulst, F.: Nonlinear Differential Equations and Dynamical Systems. Springer, Berlin, Germany (1996)
45. Farrell Helbling, E., Wood, R.J.: A Review of Propulsion, Power, and Control Architectures for Insect-Scale Flapping-Wing Vehicles. Appl. Mech. Rev. **70**, 010801 (2018). https://doi.org/10.1115/1.4038795
46. Keennon, M., Klingebiel, K., Won, H., Andriukov, A.: Development of the Nano Hummingbird: A Tailless flapping wing micro air vehicle. In: 50th AIAA Aerospace Sciences Meeting including the New Horizons Forum and Aerospace Exposition. pp. 1–24 (2012)
47. Karásek, M., Muijres, F.T., De Wagter, C., Remes, B.D.W., de Croon, G.C.H.E.: A tailless aerial robotic flapper reveals that flies use torque coupling in rapid banked turns. Science **361**, 1089–1094 (2018). https://doi.org/10.1126/science.aat0350
48. Nguyen, Q.-V., Chan, W.L.: Development and flight performance of a biologically-inspired tailless flapping-wing micro air vehicle with wing stroke plane modulation. Bioinspir. Biomim. **14**, 016015 (2018). https://doi.org/10.1088/1748-3190/aaefa0
49. Shepherd, R.F., Stokes, A.A., Freake, J., Barber, J., Snyder, P.W., Mazzeo, A.D., Cademartiri, L., Morin, S.A., Whitesides, G.M.: Using explosions to power a soft robot. Angew. Chem. Int. Ed. **52**, 2892–2896 (2013)
50. Ma, T., Zhang, H.: Reaping the potentials of nonlinear energy harvesting with tunable damping and modulation of the forcing functions. Appl. Phys. Lett. **104**, 214104 (2014). https://doi.org/10.1063/1.4879846
51. Zhang, H., Ma, T.: Roles of the Excitation in Harvesting Energy from Vibrations. PLoS ONE **10**, e0141299 (2015). https://doi.org/10.1371/journal.pone.0141299
52. Zhang, H., Ma, T., Xu, N.S.: New insights into vibration-based energy harvesting. In: Proc. SPIE 9435, Sensors and Smart Structures Technologies for Civil, Mechanical, and Aerospace Systems. p. 943504. , San Diego, CA (2015)
53. Zhang, H., Corr, L.R., Ma, T.: Issues in vibration energy harvesting. J. Sound Vib. **421**, 79–90 (2018). https://doi.org/10.1016/j.jsv.2018.01.057

54. Zhu, H.J., Sun, M.: Kinematics Measurement and Power Requirements of Fruitflies at Various Flight Speeds. Energies **13**, 4271 (2020). https://doi.org/10.3390/en13164271
55. Stramigioli, S., van Oort, G., Dertien, E.: A concept for a new Energy Efficient actuator. In: 2008 IEEE/ASME International Conference on Advanced Intelligent Mechatronics. pp. 671–675. IEEE, Xian, China (2008)
56. Seok, S., Wang, A., Chuah, M.Y., Hyun, D.J., Lee, J., Otten, D.M., Lang, J.H., Kim, S.: Design Principles for Energy-Efficient Legged Locomotion and Implementation on the MIT Cheetah Robot. IEEEASME Trans. Mechatron. **20**, 1117–1129 (2015). https://doi.org/10.1109/TMECH.2014.2339013
57. Vanderborght, B., Van Ham, R., Lefeber, D., Sugar, T.G., Hollander, K.W.: Comparison of Mechanical Design and Energy Consumption of Adaptable. Passive-compliant Actuators. Int. J. Robot. Res. **28**, 90–103 (2009). https://doi.org/10.1177/0278364908095333
58. Moon, J.-S., Bae, J.: Gait optimization and energetics of ballistic walking for an underactuated biped with knees. Nonlinear Dyn. **85**, 1533–1546 (2016). https://doi.org/10.1007/s11071-016-2777-2
59. Haberland, M., Kim, S.: On extracting design principles from biology: II. Case study—the effect of knee direction on bipedal robot running efficiency. Bioinspir. Biomim. 10, 016011 (2015). https://doi.org/10.1088/1748-3190/10/1/016011
60. Graham, R.L., Knuth, D.E., Patashnik, O.: Concrete mathematics: a foundation for computer science. Addison-Wesley, Reading, MA (1994)
61. Sun, M., Tang, J.: Unsteady aerodynamic force generation by a model fruit fly wing in flapping motion. J. Exp. Biol. **205**, 55–70 (2002). https://doi.org/10.1242/jeb.205.1.55
62. Reid, H.E., Schwab, R.K., Maxcer, M., Peterson, R.K.D., Johnson, E.L., Jankauski, M.: Wing flexibility reduces the energetic requirements of insect flight. Bioinspir. Biomim. **14**, 056007 (2019). https://doi.org/10.1088/1748-3190/ab2dbc
63. Srinivasan, M., Ruina, A.: Computer optimization of a minimal biped model discovers walking and running. Nature **439**, 72–75 (2006). https://doi.org/10.1038/nature04113
64. Margaria, R.: Biomechanics and energetics of muscular exercise. Clarendon, Oxford, UK (1979)
65. Ruina, A., Bertram, J.E.A., Srinivasan, M.: A collisional model of the energetic cost of support work qualitatively explains leg sequencing in walking and galloping, pseudo-elastic leg behavior in running and the walk-to-run transition. J. Theor. Biol. **237**, 170–192 (2005). https://doi.org/10.1016/j.jtbi.2005.04.004
66. Alexander, R.M.: A model of bipedal locomotion on compliant legs. Philos. Trans. R. Soc. Lond. B. Biol. Sci. **338**, 189–198 (1992). https://doi.org/10.1098/rstb.1992.0138
67. Myklestad, N.O.: Fundamentals of vibration analysis. Dover Publications, Mineola, NY (2012)
68. Moretti, P.M.: Modern vibrations primer. CRC Press, Boca Raton, FL (2000)
69. Ibrahimbegovic, A.: Nonlinear Solid Mechanics. Springer, Dordrecht, The Netherlands (2009)
70. Rouse, E.J., Gregg, R.D., Hargrove, L.J., Sensinger, J.W.: The Difference Between Stiffness and Quasi-Stiffness in the Context of Biomechanical Modeling. IEEE Trans. Biomed. Eng. **60**, 562–568 (2013). https://doi.org/10.1109/TBME.2012.2230261
71. Oguz, O.S., Zhou, Z., Wollherr, D.: A Hybrid Framework for Understanding and Predicting Human Reaching Motions. Front. Robot. AI. **5**, 27 (2018). https://doi.org/10.3389/frobt.2018.00027
72. van der Zee, T.J., Kuo, A.D.: The high energetic cost of rapid force development in muscle. J. Exp. Biol. 224, jeb233965 (2021). https://doi.org/10.1242/jeb.233965
73. Sclater, N., Chironis, N.P.: Mechanisms and Mechanical Devices Sourcebook. McGraw-Hill, New York, NY (2007)
74. Gomis-Bellmunt, O., Campanile, L.F.: Design rules for actuators in active mechanical systems. Springer, Dordrecht, The Netherlands (2010)
75. Pawlak, A.M.: Sensors and actuators in mechatronics: design and applications. (2017)
76. Radzevich, S.P., Dudley, D.W.: Dudley's handbook of practical gear design and manufacture. CRC Press, Boca Raton, FL (2021)
77. Dickinson, M.H., Lehmann, F.-O., Sane, S.P.: Wing Rotation and the Aerodynamic Basis of Insect Flight. Science **284**, 1954 (1999). https://doi.org/10.1126/science.284.5422.1954
78. Zhang, P., Wu, Z., Meng, Y., Tan, M., Yu, J.: Nonlinear model predictive position control for a tail-actuated robotic fish. Nonlinear Dyn. **101**, 2235–2247 (2020). https://doi.org/10.1007/s11071-020-05963-2
79. Pollard, B., Fedonyuk, V., Tallapragada, P.: Swimming on limit cycles with nonholonomic constraints. Nonlinear Dyn. **97**, 2453–2468 (2019). https://doi.org/10.1007/s11071-019-05141-z
80. Greenblatt, D., Vey, S., Paschereit, O.C., Meyer, R.: Flap Vortex Management Using Active Gurney Flaps. AIAA J. **47**, 2845–2856 (2009). https://doi.org/10.2514/1.41767
81. Ishii, H., Ting, K.-L.: SMA actuated compliant bistable mechanisms. Mechatronics **14**, 421–437 (2004). https://doi.org/10.1016/S0957-4158(03)00068-0
82. Kaynak, M., Ozcelik, A., Nourhani, A., Lammert, P.E., Crespi, V.H., Huang, T.J.: Acoustic actuation of bioinspired microswimmers. Lab. Chip. **17**, 395–400 (2017). https://doi.org/10.1039/C6LC01272H
83. Liu, J., Ruan, H.: Modeling of an acoustically actuated artificial micro-swimmer. Bioinspir. Biomim. **15**, 036002 (2020). https://doi.org/10.1088/1748-3190/ab6a61
84. Purcell, E.M.: Life at low Reynolds number. Am. J. Phys. **45**, 3–11 (1977). https://doi.org/10.1119/1.10903
85. Li, H., Qin, W.: Dynamics and coherence resonance of a laminated piezoelectric beam for energy harvesting. Nonlinear Dyn. **81**, 1751–1757 (2015). https://doi.org/10.1007/s11071-015-2104-3
86. Litak, G., Borowiec, M.: On simulation of a bistable system with fractional damping in the presence of stochastic coherence resonance. Nonlinear Dyn. **77**, 681–686 (2014). https://doi.org/10.1007/s11071-014-1330-4
87. Miwadinou, C.H., Hinvi, L.A., Monwanou, A.V., Chabi Orou, J.B.: Nonlinear dynamics of a ϕ^6-modified Duffing oscillator: resonant oscillations and transition to chaos. Nonlinear Dyn. **88**, 97–113 (2017). https://doi.org/10.1007/s11071-016-3232-0
88. Lakshmanan, M., Murali, K.: Chaos in nonlinear oscillators. World Scientific, Singapore (1996)

89. Kartashova, E.: Nonlinear resonance analysis: theory, computation, applications. Cambridge University Press, Cambridge, UK (2011)
90. Guo, M., Elmedyb, T.B., Jensen, S.H., Jensen, J.: Analysis of Acoustic Feedback/Echo Cancellation in Multiple-Microphone and Single-Loudspeaker Systems Using a Power Transfer Function Method. IEEE Trans. Signal Process. **59**, 5774–5788 (2011). https://doi.org/10.1109/TSP.2011.2168523
91. Mason, W.P., Thurston, R.N.: Physical acoustics: principles and methods. Academic Press, New York, NY (1981)
92. Takewaki, I.: Building control with passive dampers: optimal performance-based design for earthquakes. Wiley, Singapore (2009)
93. Kawai, A., Maeda, T., Takewaki, I.: Smart Seismic Control System for High-Rise Buildings Using Large-Stroke Viscous Dampers Through Connection to Strong-Back Core Frame. Front. Built Environ. **6**, 29 (2020). https://doi.org/10.3389/fbuil.2020.00029
94. Ma, X., Wilson, A., Rahn, C.D., Trolier-McKinstry, S.: Efficient Energy Harvesting Using Piezoelectric Compliant Mechanisms: Theory and Experiment. J. Vib. Acoust. **138**, 021005 (2016). https://doi.org/10.1115/1.4032178
95. Beatus, T., Cohen, I.: Wing-pitch modulation in maneuvering fruit flies is explained by an interplay between aerodynamics and a torsional spring. Phys. Rev. E. 92, 022712 (2015)
96. Ellington, C.P.: The novel aerodynamics of insect flight: applications to micro-air vehicles. J. Exp. Biol. **202**, 3439 (1999). https://doi.org/10.1242/jeb.202.23.3439
97. Ishihara, D., Horie, T.: Passive mechanism of pitch recoil in flapping insect wings. Bioinspir. Biomim. **12**, 016008 (2016). https://doi.org/10.1088/1748-3190/12/1/016008
98. Dickinson, M.H., Muijres, F.T.: The aerodynamics and control of free flight manoeuvres in Drosophila. Phil Trans R Soc B. **371**, 20150388 (2016)
99. Dickinson, M.H., Tu, M.S.: The function of dipteran flight muscle. Comp. Biochem. Physiol. A Physiol. **116**, 223–238 (1997)